HHS Public Access

Author manuscript

Sci Immunol. Author manuscript; available in PMC 2021 March 18.

Published in final edited form as:

Sci Immunol. 2020 September 18; 5(51): . doi:10.1126/sciimmunol.abb5590.

IL-21 from high-affinity CD4 T cells drives differentiation of brain-resident CD8 T cells during persistent viral infection

Heather M. Ren[1], **E. Motunrayo Kolawole**[2], **Mingqiang Ren**[3,4], **Ge Jin**[1], **Colleen S. Netherby-Winslow**[1], **Quinn Wade**[5], **Shwetank**[1], **Ziaur S. M. Rahman**[1], **Brian D. Evavold**[2], **Aron E. Lukacher**[1,*]

[1]Department of Microbiology and Immunology, Penn State College of Medicine, Hershey, PA 17033, USA.

[2]Division of Microbiology and Immunology, Department of Pathology, University of Utah, Salt Lake City, UT 84112, USA.

[3]Consortium for Health and Military Performance, Department of Military & Emergency Medicine, Uniformed Services University, Bethesda, MD 20814, USA.

[4]Henry M. Jackson Foundation for the Advancement of Military Medicine, Bethesda, MD 20814, USA.

[5]Department of Neurosurgery, Penn State College of Medicine, Hershey, PA 17033, USA.

Abstract

Development of tissue resident-memory CD8 T cells (T_{RM}) depends on CD4 T cells. In polyomavirus CNS infection, brain CXCR5^{hi} PD-1^{hi} CD4 T cells produce IL-21 and CD8 T cells lacking IL-21 receptors (IL21R$^{-/-}$) fail to become bT_{RM}. IL-21^{+} CD4 T cells exhibit elevated TCR affinity and higher TCR density. IL21R$^{-/-}$ brain CD8 T cells do not express CD103, depend on vascular CD8 T cells for maintenance, are antigen recall-defective, and lack T_{RM} core signature genes. CD4 T cell-deficient and IL21R$^{-/-}$ brain CD8 T cells show similar deficiencies in expression of genes for oxidative metabolism, and intrathecal delivery of IL-21 to CD4 T cell-depleted mice restored expression of electron transport genes in CD8 T cells to wild-type levels. Thus, high affinity CXCR5^{hi} PD-1^{hi} CD4 T cells in the brain produce IL-21, which drives CD8 bT_{RM} differentiation in response to a persistent viral infection.

*Corresponding author: Aron E. Lukacher, Department of Microbiology and Immunology, Mail Code H107, Penn State College of Medicine, 500 University Drive, Hershey, PA 17033. alukacher@pennstatehealth.psu.edu. Phone: 717-531-6521.

Author contributions: HMR and AEL contributed to the conception and design of the study and wrote the manuscript; HMR, EMK, MR, GJ, CSNW, S, and QW performed experiments, analyzed data, and performed the statistical analysis. BDE and ZSMR contributed to the conception and design of the study and provided essential resources. All authors contributed to manuscript revision, read, and approved the submitted version. Present address for S is Biocon Bristol Myers Squibb Research Centre (BBRC), Syngene Intl. Ltd., Biocon Park, Jigani link road, Bangalore, India-560100.

Competing interests: The authors declare that they have no competing interests.

Data and materials availability: All materials used in this manuscript are commercially available or available from the corresponding author upon reasonable request.

INTRODUCTION

CD8 T_{RM} sojourn permanently in non-lymphoid tissues where they act as vanguards against pathogen reencounter in mucosal and nonmucosal tissues (1–3). The most populous of the memory T cell subsets, CD8 T_{RM} are phenotypically and transcriptionally distinct from effector, effector-memory, and central-memory T cells (4–6). Moreover, T_{RM} stand armed with effector mechanisms to rapidly counter invading microbes and elicit immune defense reactions (7–9). Given their roles in anti-microbial immunity, a sizeable body of literature details the transcription factors and cytokines involved in guiding T_{RM} differentiation. A theme emerging from these studies is that the requirements for establishing T_{RM} are in large part dictated by the pathogen and infected tissue. TGFβ and IL-15 are critical cytokines for T_{RM} development and maintenance in HSV-infected skin and influenza virus-infected lung, but IL-15 is dispensable for T_{RM} differentiation in the female reproductive tract and small intestine during LCMV infection (10–14). For cutaneous vaccinia virus infection, local antigen is necessary for T_{RM} differentiation (15–17), but this is not the case for LCMV infection (1, 18). These variable requirements for cytokines and microbial antigens in the establishment of CD8 T_{RM} reinforce the concept that the pathogen and tissue microenvironment act concomitantly to control the establishment of this critical memory T cell subset in nonlymphoid tissues.

T_{RM} differentiation also requires CD4 T cell help, but are also influenced by pathogen- and tissue locale (19–21). In the brain, CD4 T cells are required for development and maintenance of antiviral CD8 T_{RM} to infection by MuPyV and *Toxoplasma gondii*, but virus-specific CD8 bT_{RM} are generated independent of CD4 T cells in LCMV CNS infection (20, 22, 23). MuPyV and *T. gondii* share the distinction of establishing persistent infections, whereas the CNS infection with LCMV (Armstrong strain) is acutely resolved. In addition, the human JCPyV polyomavirus and *T. gondii* are well-known for their association with brain pathology during AIDS, a disease defined by low CD4 T cell counts. Progressive multifocal leukoencephalopathy (PML) is the often-fatal brain demyelinating disease caused by JCPyV in the setting of AIDS and other CD4 deficiencies. More recently, PML has been diagnosed in patients treated with monoclonal antibody therapy such as natalizumab (anti-α4 integrin) and rituximab (anti-CD20) (24–26). Strong JCPyV-specific CD8 and CD4 T cell responses are associated with protection from PML, but their role and potential interactions in the CNS are unknown. In the *T. gondii* CNS infection model, knockdown of Blimp1 in CD4 T cells reversed their functional deficits and improved the function of CD8 T cells in the brain (22). We recently reported that CD8 T cells in the brains of MuPyV-infected mice require CD4 T cell help for establishing antiviral CD8 T_{RM} and endowing them with the ability to control viral reinfection (20). Further investigation is needed to define the role of CD4 T cell help in the development of CD8 bT_{RM}.

Previous studies suggest that IL-21 constitutes the requisite CD4 T cell help for CD8 T_{RM} development in the brain. IL-21 is well known as the signature cytokine produced by T_{FH} in germinal centers and is critical to driving central- and effector-memory CD8 T cell differentiation (27–30). IL-21 promotes pathogen-specific CD8 T cell function in the CNS during mouse JHMV coronavirus and *T. gondii* infections (31–33), and IL-21 has been shown to mitigate T cell exhaustion during viremic LCMV chronic infection (34–36).

Using a mouse polyomavirus (MuPyV)-CNS infection model, we demonstrate that virus-specific CD4 T cells in the brain expressing high-affinity TCRs are the sole source of IL-21, providing evidence of a link between an effector activity and TCR affinity by differentiated CD4 T cells in a non-lymphoid organ. We show that these cells exhibit a mixed T_H1/T_{FH} gene signature and that IL-21 is responsible for generating protective antiviral CD8 bT_{RM}. These findings reveal that IL-21 is critical to the CD4 T helper cell response needed for CD8 bT_{RM} development during a persistent viral CNS infection.

RESULTS

CXCR5^{hi} PD-1^{hi} MuPyV-specific CD4 T cells in the brain produce IL-21

Because CD4 T cells are required for differentiation of MuPyV-specific CD8 bT_{RM} (20), we investigated if CD4 T cells in the brain were MuPyV-specific. Mice were inoculated intracerebrally (i.c.) and brain CD4 T cells were analyzed for their ability to bind MHC-II tetramers of I-A^{b}VP1–221 (epitope from VP1, the major viral capsid protein) and I-A^{b}LT678 (epitope from the Large T antigen) (37). CD4 T cells recognizing these epitopes were detected by 6 days post-infection (dpi), with cell numbers peaking at 8–15 dpi (Fig. 1A and fig. S1A). We chose 15 dpi to characterize brain CD4 T cells because this timepoint coincided with the initial appearance of brain CD8 T cells expressing the CD103 T_{RM} marker (38).

Compared to CD4 T cells in the spleen, brain CD4 T cells expressed significantly more T-bet, pointing toward a T_H1 differentiation state for CD4 T cells infiltrating the CNS (Fig. 1B). This possibility was reinforced by evidence that the brain CD4 T cells did not consistently express Gata-3 (T_H2), RORγT (T_H17), or FoxP3 (T_{reg}) at higher levels (fig. S1B–E). Notably, the spleen and brain expression pattern for these transcription factors was similar for both MHC-II tetramer$^+$ and tetramer$^-$ CD4 T cells. A proportion of MHC-II tetramer$^+$ but not MHC-II tetramer$^-$ CD4 T cells in the brain co-expressed PD-1 and CXCR5, a phenotype consistent with T_{FH} cells (Fig. 1C). In the spleen, I-A^{b}VP1–221 but not I-A^{b}LT678 tetramer$^+$ CD4 T cells were PD-1^{hi} CXCR5^{hi} (Fig. 1C). Further evidence that these cells were T_{FH} includes the findings that CXCR5^{hi} I-A^{b}VP1–221 tetramer$^+$ CD4 T cells in the spleen expressed significantly more Bcl6 than their CXCR5^{lo} counterparts (Fig. 1D), and a larger fraction of I-A^{b}VP1–221 tetramer$^+$ CD4 T cells were CXCR5^{hi} PD-1^{hi} by 30 dpi (fig. S1F). In the brain, however, CXCR5^{hi} and CXCR5^{lo} populations of either CD4 T cell specificity expressed comparable low levels of Bcl6, and the CXCR5^{hi} fraction expressed higher levels of Blimp1, which may act to repress *Bcl6* transcription by these cells (Fig. 1D).

IL-21 is considered a signature T_{FH} cytokine, and MuPyV-specific CD4 T cells in the brain display this PD-1^{hi} CXCR5^{hi} T_{FH} phenotype, thus we used an IL21-VFP reporter mice to examine if anti-MuPyV CD4 T cells may produce IL-21. The strong fidelity of the IL21-VFP knock-in mouse used here in reporting transcription and secretion of IL-21 production by activated CD4 T cells has been previously described (39). Analysis of different immune cell populations for IL-21 production at 15 dpi identified only CD4 T cells as a distinct VFP$^+$ population (fig. S1G). Brain CD4 T cells also expressed T-bet, so we analyzed IFNγ production in parallel with IL-21 using IFNγ-eYFP reporter mice, and compared the

kinetics of cells expressing each of these cytokines during MuPyV infection. Prior to 6 dpi, few brain-infiltrating T cells can be isolated; so, T cell infiltrates were not assessed earlier than 8 dpi. Interestingly, CD4 T cells in the brain were discordant in their frequency and kinetics for IFNγ and IL-21 production (Fig. 1E). eYFP (IFNγ)$^+$ CD4 T cell frequencies peaked at approximately 25% of total CD4 T cells at 15 dpi and declined below 10% in persistently infected mice, whereas approximately 30% VFP (IL-21)$^+$ were observed from acute through persistent stages of MuPyV infection (Fig. 1E). The kinetics of IFNγ^+ CD8 T cells in the brain mirrored that of the IFNγ^+ CD4 T cells (fig. S1H). Total and virus-specific brain CD4 and CD8 T cells produced IFNγ, although CD8 T cells produced more IFNγ than CD4 T cells (Fig. 1F, **left**). The majority (> 60%) of MHC II tetramer$^+$ CD4 T cells were IL-21$^+$ (Fig. 1F, **right**). Notably, brain CD4 T cells producing IL-21 were largely PD-1^{hi} CXCR5^{hi}, further establishing that these T_{FH}-like cells produced IL-21 (Fig. 1G and fig. S1I).

Immunofluorescence microscopy of brain sections at 15 dpi illustrated CD8 T cells colocalizing with IL-21$^+$ and IL-21$^-$ CD4 T cells in the periventricular region (Fig. 1H and fig. S1J). As VFP (IL-21)$^+$ CD4 T cells aggregate in tight foci in the periventricular region, it is unlikely that IL-21 would be detected in whole brain homogenates. Collectively, these data demonstrate that CD4 T cells are the dominant source of IL-21 in the brains of MuPyV-infected mice, and that these IL-21-producing CXCR5^{hi} PD-1^{hi} cells share phenotypic characteristics with T_{FH} cells.

IL-21-producing MuPyV-specific CD4 T cells in the brain express high-affinity TCRs

MHC-II tetramers preferentially bind CD4 T cells having high-affinity TCRs, and MHC-II tetramers can underestimate frequencies of antigen-specific CD4 T cells up to nearly 10-fold (40, 41). We thus utilized 2D micropipette adhesion (2D-MP) assays to capture MuPyV-specific CD4 T cells with low-affinity TCRs. To determine 2D affinity, negatively enriched CD4 T cells from the brains or spleens of IL21-VFP reporter mice at 15 dpi were sorted as CD69$^+$ before being divided into VFP (IL-21)$^+$ and VFP (IL-21)$^-$ populations. 2D-MP assays revealed a much greater percentage of viral antigen-specific CD4 T cells than the fluorophore-tagged MHC-II tetramers. By 2D-MP assays, almost all of the IL-21-producing CD4 T cells could be accounted for as specific for the I-A^b VP1–221 or I-A^b LT678 epitopes, with approximately 60% of these CD4 T cells recognizing I-A^b VP1–221 and 40% I-A^b LT678 (Fig. 2A). These numbers were greater than the CD4$^+$ CD69$^+$ VFP$^-$ compartment, where approximately 40% and 20% bound the I-A^b VP1–221 and I-A^b LT678 monomers, respectively (Fig. 2A). Taken together, approximately 70% the CD4 CD69$^+$ T cells in the brain were specific for I-A^b VP1–221 or I-A^b LT678; these results stand in sharp relief against the fewer than 10% CD4 T cells in the brain that bind MHC-II tetramers of either specificity (Fig. 1A). 2D-MP assays detected slightly lower frequencies of MuPyV-specific CD4 T cells in the spleen than the brain. Approximately 50% and 40% of the IL-21$^+$ and 37% and 22% of the IL-21$^-$ recognized I-A^b VP1–221 and I-A^b LT678 epitopes, respectively (fig. S2A).

Because most I-A^{b}VP1–221 and I-A^{b}LT678 tetramer$^+$ CD4 T cells in the brain were VFP (IL-21)$^+$, we asked if IL-21-producing CD4 T cells had higher affinity TCRs than

nonproducers. Although the range of I-A^b VP1–221 and I-A^b LT678 spanned >1000-fold, there was a large contribution of low affinity cells in the IL-21^+ population with the highest affinity measurements found only in the IL-21^+ populations in the brain. The TCR affinity calculations confirmed that the VFP $(IL\text{-}21)^+$ CD4 T cells had higher affinity TCRs for I-A^b LT678-specific CD4 T cells and approached statistical significance for the I-A^b VP1–221 cells (Fig. 2B). In contrast, MuPyV-specific CD4 T cells in the spleen showed no statistical difference in TCR affinity between IL-21^+ and IL-21^- cells of either specificity (fig. S2B). However, the spleen follows the trend seen in the brain where the highest affinity measurements are found in the VFP $(IL\text{-}21)^+$ CD4 T cells.

We found that IL-21^+ I-A^b LT678 and I-A^b VP1–221 CD4 T cells in the brain each had higher TCR density (i.e., number of TCRs per μm^2 on the T cell surface) than the IL-21 nonproducers (Fig. 2D). In the spleen, I-A^b VP1–221-specific CD4 T cells expressed approximately twice as many TCRs per μm^2 than I-A^b LT678-specific CD4 T cells, irrespective of IL-21 production (fig. S2D). These data indicate a linkage between TCR affinity and IL-21 production by virus-specific CD4 T cells in the brain.

IL-21-producing CD4 T cells in the brain express T_H1 and T_{FH} transcriptomes

We sought to determine the extent of similarity between IL-21^+ vs. IL21^- brain CD4 T cells at transcriptional and functional levels. Using PMA and ionomycin stimulation, we observed a modest increase in the frequency of VFP^+ cells (fig. S3A). The overall frequency of VFP^+ cells remained at 30–40% of total brain CD4 T cells, suggesting that the IL-21-producing CD4 T cells differed qualitatively from the nonproducers.

That IL-21^+ and IL-21^- constituted different subpopulations of MuPyV-specific CD4 T cells in the brain received further support from gene expression profiling. RNA sequencing analysis was performed on VFP^+CD69^+ and VFP^-CD69^+ CD4 T cells FACS-sorted from brains and spleens of IL21-VFP reporter mice at 15 dpi. Based on gene sets from recently published work (42–45), clustering analysis and gene set enrichment analysis (GSEA) (46, 47), showed distinct helper T cell subtypes between IL-21^+ and IL-21^- CD4 T cells (Fig. 3A and fig. S3B & S3C). Splenic IL-21^+ CD4 T cells had a strong T_{FH} gene expression pattern, whereas the transcriptional signature of splenic IL-21^- cells most resembled that of T_{reg} (Fig 3A and fig. S3C). Irrespective of their capacity to produce IL-21, brain CD4 T cells expressed a T_H1 gene signature (Fig. 3A and fig. S3C). Cytometric bead array (CBA) for Th1/Th2/Th17 cytokines further verified this T_H1 subtype classifications inferred by GSEA for brain CD4 T cells (Fig. 3B). Brain IL-21 producers and non-producers both produced IFNγ, TNFα, and IL-2, confirming T_H1 polarization, proportionally more VFP $(IL\text{-}21)^+$ CD4 T cells were making IFNγ (fig. S3D). This observation was also appreciated in the spleen (fig. S3E).

When we compared brain VFP $(IL\text{-}21)^+$ CD4 T cells to brain VFP $(IL\text{-}21)^-$ CD4 T cells, we observed that brain IL-21 nonproducers were significantly more enriched for T_{RM} genes (Fig. 3C), although both IL-21^+ and IL-21^- CD4 T cells in the brain preferentially expressed T_{RM} signatures compared to those in the spleen (Fig. 3D). Comparing brain VFP $(IL\text{-}21)^+$ CD4 T cells to brain VFP $(IL\text{-}21)^-$ CD4 T cells also revealed that IL-21-producing CD4 T cells in the brain were significantly enriched for the T_{FH} gene set (Fig. 3C), even though

they were negatively enriched for these genes when compared to IL-21-producing CD4 T cells in the spleen (fig. S3C). We observed that several expressed genes associated with TCR signaling (*Lag3*, *Cd4*, *Cd28*, *Irf4*) were higher in the IL-21$^+$ CD4 T cells (Fig. 3D), a finding consistent with evidence that these cells had higher TCR density and higher TCR affinity. FACS analysis confirmed elevated CD4 and IRF4 levels (Fig. 3E).

Despite the sizeable transcriptomic overlap between IL-21-producing and -nonproducing CD4 T cells in brains of MuPyV-infected mice, a number of genes were differentially expressed in addition to *Il21* (Fig. 3F). That *Il21* had the highest positive differential expression in the VFP$^+$ CD4 T cells further verifies the reliability of VFP as a reporter for *Il21* expression in these mice and substantiates sample purity. Differences between these groups in expression of IL-2Rα (CD25) and FoxP3 were confirmed by FACS (Fig. 3G). Collectively, gene expression profiling analyses revealed that the CD4 T cells that produce IL-21 in brains of MuPyV-infected mice have distinct transcriptomes from those not producing IL-21.

CD8 T cells require IL-21 signaling to become brain-resident memory T cells

CD8 T cells in the brain expressed IL21(R) receptors, with peak levels at 15 dpi. In contrast, brain CD4 T cells expressed IL21R, but at lower levels and without a change in expression over the course of infection (Fig. 4A). Splenic D^b LT359 tetramer$^+$ CD8 T cells also expressed IL21Rs at substantially lower levels over 30 days of MuPyV infection (fig. S4A). Higher IL21R expression correlated directly with CD103 expression (Fig. 4B), and the significantly lower expression levels of CD103 by D^b LT359 CD8 T cells in brains of IL21R$^{-/-}$ mice is consistent with this IL21R-CD103 association (Fig. 4C) and matches our previous observation that CD4 T cell-unhelped brain CD8 T cells are CD103$^-$ (20). MuPyV levels in the brain were equivalent between WT and IL21R$^{-/-}$ mice (Fig. 4D). A similar number of brain CD4 T cells was seen between groups (Fig. S4B), suggesting that these trends were not due to differences in viral replication or CD4 T cell-insufficiency.

IL-21 has been shown to influence short-lived effector CD8 T cells (48), and here we examined whether the differences in CD8 T cells between WT and IL21R$^{-/-}$ mice could be due to altered differentiation into T_{eff} subtypes prior to recruitment into the brain. CD4 and CD8 T cells in IL21R$^{-/-}$ mice were found to enter the brain at similar frequencies as CD4 and CD8 T cells from WT mice at 8 dpi (Fig. 4E and fig. S4C). CD44^{hi} CD8 T cells were also present in the spleens of IL21R$^{-/-}$ mice at the same frequency as WT mice, but with a small decrease in the number of D^b LT359$^+$ splenic CD8 T cells was observed (fig. S4D). No differences in effector phenotypes was observed in IL21R$^{-/-}$ CD8 T cells in the brain or spleen based on KLRG1 and CD127 expression (Fig. 4F and fig. S4E). Expression levels of PD-1, IRF4, and CD69, molecules often associated with bT_{RM}, were also similar between WT and IL21R$^{-/-}$ mice at 30 dpi (fig. S4F–I).

We previously demonstrated that peripheral depletion of CD8 T cells can lead to the loss of MuPyV-specific CD8 T cells in the brains of CD4 T cell-deficient but not CD4 T cell-sufficient, mice (20). Here we depleted CD8 T cells in WT and IL21R$^{-/-}$ mice using anti-CD8β starting at 10 dpi, a time after CD8 T cells have infiltrated the brain. CD8 T cells in IL21R$^{-/-}$ mice, but not WT mice, were completely depleted in the brain by anti-CD8β (Fig.

4G), whereas CD8 T cells were efficiently depleted in spleens off both WT and IL21R$^{-/-}$ mice (fig. S4J). To determine whether the IL21R$^{-/-}$ CD8 T cells were intravascular and directly exposed to anti-CD8β, anti-CD45 i.v. was injected 3 min prior to euthanization. As previously observed (20), < 5% D^{b} LT359^{+} WT CD8 T cells in the brain were CD45-i.v.$^{+}$ in both WT and IL21R$^{-/-}$ mice (fig S4K). CD45-i.v.$^{+}$ cells had lower expression of the bT$_{RM}$ markers CD103, CD69, PD-1, and CXCR5 (fig. S4L), further showing that these cells were vascular and not T$_{RM}$. RNA sequencing of FACS-sorted D^{b} LT359 tetramer^{+} CD8 T cells from brains of WT and IL21R$^{-/-}$ mice confirmed a role of IL-21 signaling in the development of brain-resident CD8 bT$_{RM}$ during infection (Fig. 4H). GSEA for expression of core T$_{RM}$ cell genes (5), revealed these genes are negatively enriched in brain CD8 T cells from IL21R$^{-/-}$ mice (Fig. 4H).

We reported that MuPyV-specific CD8 T cells in brains of persistently infected WT mice had superior recall responses to antigen rechallenge than those in CD4 T cell-depleted mice (20). Likewise, D^{b} LT359^{+} CD8 T cells in brains of WT mice showed significantly higher expansion compared with IL21R$^{-/-}$ mice after rechallenge with a recombinant VSV encoding the D^{b} LT359 epitope (Fig. 4I and fig. S4M).

IL-21 signaling for development of brain-resident memory is CD8 T cell-intrinsic.

To determine whether these IL21R signaling defects were intrinsic to MuPyV-specific CD8 T cells, we created WT/IL21R$^{-/-}$ mixed bone marrow (BM) chimeras (Fig. 5A). After engraftment, we saw an approximately 85:15 ratio of WT:IL21R$^{-/-}$ T cells in the blood. This ratio remained in the spleen after infection, but not in the brain in which the ratio was ~99:1 WT:IL21R$^{-/-}$ (Fig. 5B). Of the few IL21R$^{-/-}$ CD8 T cells detected in the brain, a small fraction were CD103^{+} (Fig. 5C), and they expressed lower levels of CD69 (Fig. 5D) than the IL21R^{+} CD8 T cells. As the populations of IL21R$^{-/-}$ CD8 cells in the brains of BM chimeric mice were so small, we injected anti-CD8 i.v. prior to euthanization to assess whether these cells may represent vasculature contamination. We also included a group of WT:IL21R$^{-/-}$ mixed BM chimeric mice at 8 dpi to determine if IL21R$^{-/-}$ CD8 T cells that were recruited to the brain, but not maintained, were situated in the CNS vasculature. >20% of IL21R$^{-/-}$ CD8 T cells were i.v.$^{+}$ (Fig. 5E), indicating that a sizeable portion of these cells were in the vasculature. Intravascular CD8 T cells expressed little to no CD69 than the CD8 T cells in the brain parenchyma (fig. S4L). Together, these data indicate that a probable reason for the lower levels of CD69 expression on IL21R$^{-/-}$ CD8 T cells in the BM chimeric mice was contamination by CD69^{lo} cells from the vasculature. In addition, IL21R$^{-/-}$ CD8 T cells in the BM chimeric mice were in the brain at the same ratio as in the spleen at 8 dpi, but this brain: spleen ratio was decreased at 30 dpi (Fig. 5F), further supporting the conclusion that the IL21R$^{-/-}$ CD8 T cells entered the brain, but were not maintained. The preference for IL21R^{+} CD8 T cells in the brain argues that IL-21 signaling in CD8 T cells is required for survival or recruitment to the CNS. Moreover, differences in expression of CD103 and CD69 between WT vs IL21R$^{-/-}$ CD8 T cells indicate that IL-21 signaling is intrinsic to the CD8 T cells undergoing T$_{RM}$ differentiation.

IL-21 signaling controls oxidative metabolism by MuPyV-specific CD8 T cells in the brain

We investigated whether CD4 T cells and IL-21 altered the metabolic state of CD8 T cells in the brains of mice persistently infected with MuPyV. RNA sequencing analysis was performed on CD8 T cells FACS-sorted from brains of WT mice, CD4 T cell-depleted mice (anti-CD4 started at 6 dpi to mitigate potential effects on CD8 T cell priming/expansion), and IL-21R$^{-/-}$ mice (fig. S5A). Metascape pathway analysis (49) of the significantly downregulated genes in CD8 T cells from IL21R$^{-/-}$ and CD4 T cell-depleted mice compared with those from WT mice revealed deficiencies in oxidative phosphorylation and other metabolic pathways (fig. S5B). GSEAs using gene sets from the Molecular Signatures Database (MSigDB, gsea-msigdb.org/gsea/msigdb) corroborated this pathway analysis, further showing that the top gene set negatively enriched in CD8 T cells from CD4 T cell-depleted and IL21R$^{-/-}$ mice were oxidative phosphorylation genes (Fig. 6A). Using a gene set for mitochondrial energy metabolism genes (6), we also found that both the CD4 T cell-depleted and IL21R$^{-/-}$ transcriptomes of the CD8 T cells were negatively enriched for genes within the electron transport chain (ETC) (Fig. 6B & E).To validate these RNAseq results, we used FACS assays to assess at the single-cell level nutrient uptake and mitochondrial fitness by 2-NBDG uptake and Mitotracker dye staining, respectively. Fewer brain CD8 T cells from IL21R$^{-/-}$ mice were double-positive for 2-NBDG and Mitotracker compared with WT CD8 T cells, whether stimulated with LT359 peptide or left unstimulated (Fig. 6C). This was also seen in CD8 T cells isolated from our WT/IL21R$^{-/-}$ BM chimeras, supporting the idea that these defects are due to cell intrinsic defects in IL21R signaling (Fig. 6D).

We next asked if exogenous IL-21 could complement the defect in oxidative metabolism imposed on brain CD8 T cells by CD4 T cell deficiency. Mice were depleted of CD4 T cells starting 6 dpi and, from 8–30 dpi, IL-21 or artificial CSF vehicle was delivered continuously (Fig. 6F). CD8 T cells were FACS-sorted from brains at 30 dpi and analyzed for expression of genes in the ETC that were most significantly depressed in IL21R$^{-/-}$ and CD4 T cell-depleted mice (Fig. 6E). IL-21 supplementation restored to WT levels transcripts for *Ndufa3* (Complex I), *Ndufb10* (Complex I), and *Cox6c* (Complex IV) to WT levels relative to significantly reduced levels measured in CD4 T cell-deficient mice (Fig. 6F). These findings strongly support the conclusion that IL-21 is the essential help provided by CD4 T cells to drive differentiation of CD8 bT$_{RM}$ during MuPyV CNS infection.

DISCUSSION

CD8 T$_{RM}$ are sentinels of viral reencounter at mucosal portals of entry, but are also involved in maintaining dormancy of persistent viral infections (50). For MuPyV, a persistent mouse pathogen, CD4 T cells are essential for CD8 T$_{RM}$ differentiation in the brain (20). Here, we identify IL-21 as the central component of virus-specific CD4 T cell help that establishes anti-MuPyV CD8 bT$_{RM}$, rendering them refractory to peripheral CD8 T cell depletion, and driving expression of the T$_{RM}$ marker CD103 and antigen recall capability. We stratified the IL-21-producing virus-specific “helper” virus-specific CD4 T cells into those bearing a CXCR5^{hi} PD-1^{hi} phenotype, mixed T$_H$1-T$_{FH}$ polarization, and expressing high-affinity TCRs. The proximity of CD8 and VFP(IL-21)$^+$ CD4 T cells within periventricular foci of mice also supports the hypothesis that CD4-CD8 interactions that promote CD8 T cell

differentiation into T_{RM}. CD8 T_{RM} are oxidative metabolism-biased (51, 52), and in the absence of CD4 T cells or IL21R signaling, brain CD8 T cells in MuPyV-infected mice exhibit deficiencies in oxidative metabolism. IL-21 delivery to the CNS restored deficits in ETC gene expression by brain anti-MuPyV CD8 T cells in CD4 T cell-depleted mice, further demonstrating that IL-21 is involved in providing help from CD4 T cells that is associated with shift toward oxidative metabolism in CD8 bT_{RM}. Collectively, these findings demonstrate that IL-21 is a key component of CD4 T cell help for CD8 bT_{RM} development during a persistent viral CNS infection.

Recent work by some of our group showed that TCR affinity of naïve CD4 T cells correlates with their ability to produce IL-2 and the fate decision to develop into IL-21-producing T_{FH} cells (53). Our data are congruent with these findings in several aspects. MuPyV-specific CD4 T cell IL-21 producers in the brain have higher affinity TCRs and express more *Icos*, whereas IL-21 nonproducers express higher levels of *Il2ra* and CD25. These similarities raise the interesting possibility that naïve IL-2-producing CD4 T cells are progenitors of the IL-21-producing MuPyV-specific CD4 T cell in the CNS. These data also implicate elevated TCR signal strength in the genesis of IL-21-producing CD4 T cells in the CNS. However, we observed that a proportion of both IL-21-producing and nonproducing brain CD4 T cells also produce IL-2 and express Blimp1. Despite the transcriptional and phenotypic overlap between the CD4 T cell IL-21 producers and T_{FH}, the IL-21-producing CD4 T cells are T_H1-polarized in a nonlymphoid tissue environment (i.e., brain) that harbors high levels of viral antigen. High antigen levels likely enforce high Blimp1 expression and reciprocal downregulation of Bcl6. Bcl6 expression in the brain VFP^+ (IL-21-producing) CD4 T cells is lower than Bcl6 expression in VFP^+ CD4 splenocytes, but Bcl6 gene expression is positively enriched in brain VFP^+ CD4 T cells compared to brain VFP^- (GSEA RMS = 0.9798, ES = 0.22). These differences are in line with the prevailing concept that IL-2 receptor signaling and Bcl6 expression represent divergent memory programs for effector and central T cell memory, respectively (54). This programming difference may also explain why brain VFP^+ CD4 T cells are negatively enriched for T_{RM} genes compared to VFP^- CD4 T cells, because T_{CM} have less overlap with T_{RM} than T_{EM}.

The initial MuPyV brain infection is controlled under CD4 T cell-deficient (20) and IL21R $^{-/-}$ conditions, indicating that effector functionality of unhelped CD8 T cells remains intact. However, in contrast to virus-specific CD8 T cells in WT mice, anti-MuPyV CD8 T cells in CD4 T cell-depleted and $IL21R^{-/-}$ mice rely on circulating CD8 T cells for maintenance in the brain (Fig. 4G) and exhibit poor ability to expand upon antigen rechallenge (Fig. 4I). Stable cell numbers in the face of cell loss in the circulating population is a key characteristic that defines these CD8 T cells as bT_{RM}. CD8 T cells have been shown to limit reactivation of HSV infection (55), and may operate similarly against MuPyV infection to prevent viral resurgence during persistence. Thus, should immune homeostasis be disrupted peripherally, brain CD8 T cells likely will fail to differentiate into bT_{RM} capable of controlling resurgent PyV infection. CD4 T cell deficiency is associated with PML and may underlie loss of CD8 T cell-mediated protection against JCPyV-infected glia (56–58). Support for this scenario comes from the lower level of proliferation by MuPyV-specific CD8 T cells upon i.c. delivered antigen rechallenge (Fig. 4I).

T cells at different states of differentiation vary in their utilization of aerobic glycolytic vs. oxidative respiration and ample evidence points toward metabolism directing T cell differentiation programs (51, 52, 59, 60). Recent studies document that CD8 T_{RM}, like naïve T cells, preferentially utilize oxidative metabolism, whereas effector T cells engage glycolytic metabolism (51, 61). Survival of CD8 T_{RM} in the skin requires exogenous lipid uptake and fatty acid oxidation (FAO) as its preferred metabolic pathway (62, 63). CD8 T_{RM} infiltrating gastric adenocarcinomas similarly rely of fatty acid oxidation for their survival, with PD-1 blockade promoting lipid uptake (64). An important consideration with the current data on immunometabolism of CD8 T_{RM} is that most of these studies focus on CD8 T_{RM} in the skin or mucosal barrier sites (65). Neurons are terminally differentiated, sensitive to injury, and often irreplaceable. Thus, CD8 T cells in the brain must balance viral control against immunopathology, while CD8 T cells in the skin and other mucosal barrier sites are not so constrained. This may account for differences generally seen between various T_{RM} markers on the CD8 T cells in the skin vs. brain - CD103 and granzyme B are expressed by almost all skin T_{RM}, but only by a fraction of bT_{RM}. Some of the byproducts of FAO damage astrocytes and other brain-resident cells (66). It is not known whether CD8 bT_{RM} use free fatty acids as their energy source or if they, like nonimmune cells in the brain, prefer glucose. The limited data available on effects of IL-21/IL21R signaling in CD8 T cells metabolism point to glucose as the primary external source of metabolic fuel (67). CD8 T cells exposed to IL-21 in vitro shift their metabolic profile from aerobic glycolysis to fatty acid oxidation, but decrease their incorporation of BIODIPY FL C_{16} (fluorescently labeled fatty acid) (67). This suggests that IL-21 directs CD8 T cells to preferentially use intrinsic (rather than extrinsic) fatty acids to fuel FAO. Similar to our data, Cullen et. al. observed that CD4 T cell-unhelped lung CD8 T_{RM} are negatively enriched for OX-PHOS genes by GSEA during influenza infection, as well as finding that these cells incorporated less 2-NBDG incorporation after stimulation than helped CD8 T_{RM} (21). Collectively, this literature and our findings raise the important point that the metabolic pathways utilized by T_{RM} may be tissue- and/or virus-dependent.

Our findings extend recent evidence linking TCR: Peptide–MHC (pMHC) affinity with cytokine production in naïve CD4 T cells in lymphoid tissues to virus-specific CD4 T cells in the CNS. Specifically, we show that IL-21-producing CD4 T cells express higher affinity TCRs than the IL-21 nonproducers. For the VFP $(IL\text{-}21)^+$ CD4 T cells, there appear to be three populations of varying TCR affinities for I-A^b VP1–221-specific CD4 T cells and two populations for the VFP $(IL\text{-}21)^+$ I-A^b LT678 CD4 T cells (Fig. 2B). This larger spread in the I-A^b VP1–221 population likely contributes to the higher *p*-value and failure to achieve statistical significance. Another possibility is that these data point toward fine delineations between TCR affinities and effector functions. The histograms of VFP expression in Fig. 1F suggest that there are CD4 T cells producing high and low levels of IL-21. Perhaps those CD4 T cells with the highest affinity TCRs correlate with cells having the highest gMFI of VFP (i.e., the most IL-21 production). The larger fraction of $IFN\gamma^+$ cells in the VFP $(IL\text{-}21)^+$ CD4 T cells appears at odds with the CBA data showing more IFNγ in the media of VFP $(IL\text{-}21)^-$ CD4 T cells (Fig. 3B and fig. S3A). Differences in T cell stimulation methodology and assay readouts likely account for this apparent discrepancy. It is also interesting to consider whether the higher affinity cells may be IL-21 and IFNγ co-

producers. This possibility is supported by evidence that MHC-II tetramers bind the highest affinity TCRs on CD4 T cells (40) and our data showing an overlap between these two cytokines in the MHC-II tetramer$^+$ populations (Fig. 1F).

In summary, evidence presented here shows that IL-21 produced by CD4 T cells provides the environmental context for development of CD8 T_{RM} in the brain during persistent viral infection. Strong CD8 T cell responses to JCPyV are linked to favorable outcomes in PML patients (57), and CD4 T cell insufficiency predisposes to PML (68). Our finding that IL-21 produced by CD4 T cells drives development of protective CD8 bT_{RM} offers a unifying framework for these associations and presents new therapeutic opportunities for PML.

Study Design

The purpose of this study was to elucidate a mechanism for CD4 T cell help to CD8 T cells in the brain to persistent virus infection. To define the nature of this CD4 T cell help, we characterized MuPyV-specific brain CD4 T cells using MHC-II tetramers and common flow cytometry markers. IFNγ-eYFP and IL21-VFP reporter mice were used to determine the IFNγ and/or IL-21 production profile during MuPyV brain infection. 2D-MP and RNAseq on FACS-sorted VFP$^+$ and VFP$^-$ CD4 T cells from IL21-VFP mice allowed us to compare the TCR:pMHC affinities and gene expression profiles of IL-21 producers to IL-21 nonproducers. To determine if signaling through the IL21R was required by the CD8 T cells for bT_{RM} status, we assessed CD8 T cells in IL21R$^{-/-}$ conditions (global and CD8 T cell intrinsic using 1:1 mix of CD45.1/CD45.2 WT:CD45.2 IL21R$^{-/-}$ BM chimeras). To further confirm that IL-21 plays a role in CD4 T cell help to the CD8 T cells, we compared the transcriptomes of brain CD8 T cells from WT, CD4 T cell-depleted (unhelped), and IL21R$^{-/-}$ mice. The ALZET osmotic pump and brain infusion kits enabled us to deliver exogenous IL-21 directly into the lateral left ventricle of CD4 T cell-depleted mice over a time period of 22 days to determine if IL-21 could rescue deficits in CD8 T cells in the brains of CD4 T cell-insufficient mice.

MATERIALS AND METHODS

Mice

C57BL/6NCr (stock #OIC55) and B6-ly5.1/Cr (stock #564) mice were purchased from the Frederick Cancer Research and Development Center of the National Cancer Institute (Frederick, MD). IL21R$^{-/-}$ (Stock #015505-UCD) (69) mice were purchased from the Mutant Mouse Resources and Research Centers at the University of California-Davis (Davis, CA) and backcrossed to the C57BL/6 background. IFNγ-eYFP (Stock #017581) (70) and IL21-VFP (stock #030295) (39) mice were purchased from The Jackson Laboratory (Bar Harbor, ME). All mice were housed in accordance with the guidelines of the Institutional Animal Care and Use Committees and the Department of Comparative Medicine at the Pennsylvania State University College of Medicine. The Pennsylvania State University College of Medicine Animal Resource Program is accredited by the Association for Assessment and Accreditation of Laboratory Animal Care International (AAALAC). The Pennsylvania State University College of Medicine has an Animal Welfare Assurance on file

with the National Institutes of Health's Office of Laboratory Animal Welfare; the Assurance Number is A3045–01.

Infections

7–12 week-old anesthetized mice were i.c. inoculated by injecting the right frontal lobe with 6×10^5 PFU of MuPyV strain A2 in 30 μL of DMEM as described (38). VSV.LT359 rechallenge experiments were performed by i.c. injection of 2×10^4 PFU of VSV.LT359 in 30 μL DMEM at 30 dpi of MuPyV.

Bone marrow chimeric mice

Protocol was modified from the Zajac group (30). B6-ly5.1/Cr (CD45.1) mice were lethally irradiated (500 rads x 2, 4 h apart). Femurs from C57BL/6NCr x B6-ly5.1/Cr F1 (WT, CD45.1/CD45.2) and IL21R$^{-/-}$ (CD45.2) mice were flushed with a 26G needle. BM cells were pushed through a 70 mm strainer and resuspendened in ACK lysis buffer to remove RBCs. Remaining cells were resuspended in CD5 microbeads (Miltenyi Biotec, Bergisch Gladbach, Germany) and pushed through a LD column (Miltenyi Biotec, Bergisch Gladbach, Germany) to remove mature T cells. Flow-through cells were resuspended in PBS and counted to achieve a 1:1 mix of WT:IL21R$^{-/-}$ at a total cell concentration of 2×10^7 cells/mL. 500 μL of the 1:1 mix was i.v. injected into the tail veins of the irradiated SJL recipients. Eight weeks post-transfer, recipient mice were checked for engraftment by collecting blood from the submandibular vein.

T cell depletion

CD4 T cells were depleted with 250 μL of monoclonal rat anti-CD4 (GK1.5) at 1 mg/mL in sterile PBS i.p. CD8 T cells were depleted with 250 μL of monoclonal rat anti-CD8β (H35) at 1 mg/mL in sterile PBS i.p. CD4 T cell depletion began at 6 dpi and CD8 T cell depletion began at 10 dpi. To ensure T cells were depleted within the first week, a second dose was given 48 h after the first dose. Doses were given weekly thereafter. Mice were checked for depletion by collecting blood from the submandibular vein at 8 or 12 dpi to check CD4 or CD8 T cell depletion respectively. <1% of live blood cells positive for CD4 (RM4–5) or CD8α (53–6.7) was considered adequate depletion as this was >10-fold decrease in staining compared to Rat IgG treated.

Intraventricular cannulation

C57BL/6Cr mice were depleted of CD4 T cells as described above. One day prior to surgery, ALZET mini-osmotic pumps (Model 2004, DURECT Corporation, Cupertino, CA) were filled with 0.5 μg/mL of recombinant mouse IL-21 (BioLegend, San Diego, CA) in artificial cerebral spinal fluid (aCSF) (aCSF formula outlined on ALZET website, DURECT Corporation, Cupertino, CA) or aCSF only, connected to brain infusion cannulas (ALZET Brain Infusion Kit 3), and activated at 37°C in sterile PBS (Baxter Healthcare Corporation, Deerfield, IL) per manufacturer's instructions. At 8 dpi, surgeries were performed as described (71). Osmotic pumps were implanted subcutaneously. A small hole was drilled into the skull 0.2 mm lateral and 0.1 mm posterior to Bregma. The needle of the cannula was placed into this hole and the cannula was secured to the skull with Loctite 454 instant

adhesive to deliver the pump contents into the left lateral ventricle for 22 days with a flow rate of 0.25 μL/hr. Skin was sutured over the cannula and topical antibiotics (SMZ/TMP) were applied to keep the incision clean. Delivery of aCSF +/− IL-21 to the lateral ventricle was confirmed by measuring the weight of the pump before and after placement into the mice.

Quantitation of MuPyV Genomes and LT-Ag mRNA

TaqMan real-time PCR was performed in an ABI StepOnePlus (Applied Biosciences) with 10 ng of template DNA. DNA was purified from tissues by homogenization in nuclear lysis solution (Promega, Madison, WI) followed by incubation with protein precipitation solution (Promega, Madison, WI) to obtain DNA in the supernatant. The supernatant was then incubated with isopropanol to precipitate the DNA. The precipitated DNA was washed in ethanol and dissolved in molecular grade water. Primers and amplification parameters are previously described (72).

Cell isolation

For isolation of lymphocytes, mice were euthanized, and brains and spleens were removed. Brains and spleens were minced and digested with Collagenage I (40mg/100ml) for 20 minutes at 37° C. Brain homogenates were subjected to a two-step percoll gradient (44%/66%) to remove myelin and cell debris. Cells were collected from the 44%/66% interface and washed with 5% FBS DMEM before flow cytometry staining.

Flow cytometry

CD8 and CD4 T cell gating strategies are shown in fig. S6. MHC-II tetramer staining of CD4 T cells was performed as previously described (37). Phycoerythrin-conjugated I-A^b VP1–221–235, I-A^b LT678–690 and I-A^b hCLIP tetramers (NIH Tetramer Core Facility, Atlanta GA) were diluted to 8 μg/mL per 1×10^6 spleen or brain cells in 5% FBS DMEM and incubated with the cells at 37°C for 1.5 h. As each sample required separate flow panels for each of the three tetramers and < 10% of the CD4 T cells in the brain bound tetramer, mice were pooled in groups of three to ensure the sizes of the MHC-II $tetramer^+$ populations isolated from the brains were sufficiently robust for statistical analysis. After the CD4 tetramer staining, spleen and brain cells were exposed to Fixable Viability Dye (eBioscience, San Diego, CA) prior to staining for CD8 tetramers, surface molecules, and/or intranuclear molecules. Allophycocyanin-conjugated D^b LT359–638 tetramers (NIH Tetramer Core Facility, Atlanta, GA) and antibodies to the following molecules were used: CD8α (53–6.7), CD4 (RM4–5), CD44 (IM7), CD11b (M1/70), CD45 (30-F11), CD45.2 (104), CD69 (H1.2F3), CD103 (M290), IL21R (4A9), CXCR5 (2G8), Blimp-1 (5E7), Bcl-6 (K112-g1), IFN-rdrd (XMG1.2), and IL-2 (JES6–5H4) were purchased from BD Biosciences (San Diego, CA); PD-1 (RMP1–30), Streptavidin, and IRF4 (3E4) were purchased from eBioscience (San Diego, CA); and CD25 (3C7), CD45.1 (A20), Tbet (4B10), FoxP3 (MF-14), GATA3 (16E10A23), GFP (FM264G), and TNFα (MP6-XT22) were purchased from BioLegend (San Diego, CA). To identify cells in the brain vasculature, mice were injected i.v. with 30 μg of CD45 (30-F11) or CD8α (53–6.7) 3 min prior to euthanization (73). Prior to intranuclear staining, cells were fixed and permeabilized with eBioscience Fixation/Perm (eBioscience, San Diego, CA). FACS metabolic assays were performed as

described on the Greg Delgoffe laboratory website (http://www.delgoffe-lab.com/). Briefly, CD8 T cells were incubated for 30 m at 37°C in serum-free RPMI containing 100 uM of the fluorescent glucose analog 2-NBDG (Cayman Chemical, Ann Arbor, MI), or 4 h with LT359 peptide (Peptide 2.0 Inc., Chantilly, VA) and brefeldin A (BD Biosciences, San Diego, CA). During surface staining, 10 nM MitoTracker Deep Red (Invitrogen, Carlsbad, CA) was added and live cells were run on the flow cytometer immediately after the final wash. Samples were acquired on an LSR II or LSR Fortessa (BD Biosciences, San Diego, CA) and analyzed using FlowJo software (Tree Star, Ashland, OR).

Intracellular cytokine stimulation

Brain and spleen cells were stimulated with 1 μM of PMA and ionomycin or LT359 peptide for 4 h in the presence of brefeldin A, stained for viability and surface markers, fixed and permeabilized with CytoFix/CytoPerm (BD Biosciences, San Diego, CA), then stained for intracellular IFNγ, TNFα, and IL-2. Staining for these cytokine antibodies in the absence of peptide was <1% $CD4^+CD44^{hi}$- or $CD8^+CD44^{hi}$-gated cells. Samples were acquired on an LSR II or LSR Fortessa (BD Biosciences) and analyzed using FlowJo software (Tree Star, Ashland, OR).

Cytometric bead array

Sorted (BD FACSAria, BD Bioscience, San Diego, CA) VFP^+ and VFP^- CD4 T cells from brains and spleens of IL21-VFP reporter mice at 15 dpi were incubated with CD3/CD28 dynabeads (Thermo Fischer Scientific, Waltham, MA) for 24 h at 37°C in 200 μL of 5% FBS DMEM. After 24 h, 50 μL of media was used for the BD CBA Mouse Th1/Th2/Th17 Cytokine Kit (BD Biosciences, San Diego, CA) following the manufacturer's instructions.

2D-Micropipette cell adhesion assay

CD4 T cells from brains and spleens of IL21-VFP mice were enriched for using magnetic bead-based negative selection kits (STEMCELL Technologies Inc., Vancouver, BC). They were then sorted on a BD FACSAria II (BD Biosciences) based on expression of CD69 and VFP (IL21) to obtain a $CD69^+VFP^+$ population and a $CD69^+VFP^-$ population. The relative 2D affinity of polyclonal I-A^b LT678 or VP1–122 specific $CD4^+$ $CD69^+$ T cells from either the brain or spleen of MuPyV infected mice was measured using the previously characterized 2D-MP (38, 40, 74).

Immunofluorescence microscopy

Anesthetized mice were transcardially perfused with PBS followed by 10% Formalin. Skulls containing whole brains where kept overnight at RT in 10% Formalin. Brains were removed the following day and incubated in 10% Formalin overnight at 4C and then dehydrated in 30% sucrose for 3 days. Brains were hemisected sagittally, frozen in OCT, and cut in 12 μm sagittal sections using a Leica CM1860 UV cryostat (Leica Biosystems, Wetzlar, Germany). Primary antibodies include: Goat anti-GFP (Abcam, Cambridge, UK), Rabbit anti-CD8α (Sino Biological Inc., Beijing, China) and anti-CD4-PE (GK1.5, BioLegend). Secondary antibodies against goat (bovine anti-goat AF488) and rabbit (donkey anti-rabbit AF647)

were purchased from Jackson ImmunoResearch (West Grove, PA). Images were acquired using a Leica DM4000 B LED microscope (Leica Biosystems, Wetzlar, Germany).

RNA isolation and RNA sequencing library generation

$CD69^+$ CD4 T cells from the brains and spleens of IL21-VFP MuPyV-infected mice at 15 dpi were sorted into VFP^+ ($IL\text{-}21^+$) and VFP^- populations to purity (enriched >92% based on post-sort analysis) using a BD FACSAria II (BD Biosciences, San Diego, CA). Likewise, D^b $LT359^+CD103^-$ CD8 T cells from the brains of C57BL/6NCr (WT), C57BL/6NCr CD4 T cell-depleted, and $IL21R^{-/-}$ MuPyV-infected mice at 30 dpi were sorted to purity (enriched >94% based on post-sort analysis) using a BD FACSAria II (BD Biosciences, San Diego, CA). RNA was isolated from these samples using Trizol reagent (Ambion Life Technologies, Austin, TX). Samples with high-quality RNA (RNA integrity number >7.0) were used for library preparation. The mRNA was obtained from total RNA after depletion of rRNA using RiboGone-Mammalian Kit (Takara Bio Inc., Liaoning, China) and then purified using the AMPure PCR Purification Kit (Beckman Coulter, Indianapolis, IN). cDNA libraries were subsequently prepared using the SMARTer Stranded RNA-seq Kit (Takara Bio Inc., Liaoning, China). Libraries were sequenced on an Illumina NextSeq platform using a 75-cycle single-end high-output sequencing run (Illumina, San Diego, CA).

RNAseq data analysis

RNAseq reads were demultiplexed (bcl2fastq), and FASTQ files were aligned to mouse genome GRCm38.96 (www.ensembl.org) using the STAR Aligner v2.5 (github.com/alexdobin/STAR) with 2-pass method. Sequenced read quality was checked with FastQC (bioinformatics.babraham.ac.uk/projects/fastqc). The gene expression profiles were quantified using Bioconductor R package of DESeq2 version 1.26 to get the Reads Per Kilobase of transcript per Million mapped reads (RPKM) for direct comparison between samples, as described (bioconductor.org/packages/devel/workflows/vignettes/rnaseqGene/inst/doc/rnaseqGene.html). Significant genes were determined based on a False Discovery Rate (FDR) threshold of 5% (<0.05). Volcano plots were generated to visualize significance and fold changes of gene expression obtained from RNAseq data. In the volcano plot, log fold changes of normalized gene expression in the first group compared with the second group were used as an x-axis and -log10 Q values were used as a y-axis. The gene set enrichment analysis (GSEA) was performed as outlined on the Broad Institute website (broadinstitute.org/gsea/index.jsp).

Statistical analysis

p values were determined by paired Wilcoxon ranked test, unpaired Mann Whitney test, or one-way or two-way ANOVA using GraphPad Prism software (La Jolla, CA). All *p* values ≤ 0.05 were deemed significant.

Supplementary Material

Refer to Web version on PubMed Central for supplementary material.

Acknowledgments:

We thank Matthew Lauver for helpful discussions and editing the manuscript, and Allan Zajac (University of Alabama at Birmingham) for the protocol for generating bone marrow chimeric mice and for helpful discussions. We thank the Penn State College of Medicine Flow Cytometry Core Facility staff, N. Sheaffer, J. Bednarczyk, J. Vogel, and J. Zhang, and Craig Praul, the Director of the Penn State University Genomics Core Facility in the Huck Institutes of Life Sciences for use of services and expertise. The authors also thank the National Institutes of Health Tetramer Core Facility (Emory University) for providing all of the pMHC monomers and tetramers used in this study, and the University of Utah.

Funding: Research reported in this publication was supported by the National Institute of Neurological Disorders and Stroke and the National Institute of Allergy and Infectious Diseases of the National Institute of Health under award numbers R01NS088367 and R01NS092662 to AEL, R01AI147641to BDE, R01AI091670 to ZSMR, F32NS106730 to CSNW, and F31AI142997 to HMR. The content is solely the responsibility of the authors and does not necessarily represent the official views of the National Institutes of Health. This work was also supported by the Penn State College of Medicine Finkelstein Memorial Student Research Award to HMR, and the University of Utah Flow Cytometry Facility in addition to the National Cancer Institute through the Award Number 5P30CA042014–24 and the National Center for Research Resources of the National Institute of Health under Award Number 1S10RR026802–01.

REFERENCES

1. Masopust D, Choo D, Vezys V, Wherry EJ, Duraiswamy J, Akondy R, Wang J, Casey KA, Barber DL, Kawamura KS, Fraser KA, Richard J, Brinkmann V, Butcher EC, Newell KA, Ahmed R. Dynamic T cell migration program provides resident memory within intestinal epithelium. J. Exp. Med 207, 553–564 (2010). [PubMed: 20156972]
2. Wakim LM, Woodward-Davis A, Bevan MJ. Memory T cells persisting within the brain after local infection show functional adaptations to their tissue of residence. Proc. Natl. Acad. Sci. (USA) 107, 17872–9 (2010). [PubMed: 20923878]
3. Wakim LM, Woodward-Davis A, Liu R, Hu Y, Smyth G, Bevan MJ, Villadangos J, Smyth G, Bevan MJ. The molecular signature of tissue resident memory CD8 T cells isolated from the brain. J. Immunol 189, 3462–71 (2014).
4. Mackay LK, Minnich M, Kragten NAM, Liao Y, Nota B, Seillet C, Zaid A, Man K, Preston S, Freestone D, Braun A, Wynne-Jones E, Behr FM, Stark R, Pellicci DG, Godfrey DI, Belz GT, Pellegrini M, Gebhardt T, Busslinger M, Shi W, Carbone FR, van Lier RAW, Kallies A, van Gisbergen KPJM. Hobit and Blimp1 instruct a universal transcriptional program of tissue residency in lymphocytes. Science 352, 459–463 (2016). [PubMed: 27102484]
5. Milner JJ, Toma C, Yu B, Zhang K, Omilusik K, Phan AT, Wang D, Getzler AJ. Runx3 programs $CD8^+$ T cell residency in non-lymphoid tissues and tumours. Nature 552, 253–257 (2017). [PubMed: 29211713]
6. Li C, Zhu B, Son YM, Dong H, Li C, Zhu B, Son YM, Wang Z, Jiang L, Xiang M, Ye Z, Beckermann KE. The transcription factor Bhlhe40 programs mitochondrial regulation of resident $CD8^+$ T cell fitness and functionality. Immunity 51, 491–507 (2019). [PubMed: 31533057]
7. Schenkel JM, Fraser KA, Vezys V, Masopust D. Sensing and alarm function of resident memory $CD8^+$ T cells. Nat Immunol 14, 509–513 (2013). [PubMed: 23542740]
8. Schenkel JM, Fraser K. a, Beura LK, Pauken KE, Vezys V, Masopust D, Resident memory CD8 T cells trigger protective innate and adaptive immune responses. Science 346, 98–101 (2014). [PubMed: 25170049]
9. Ariotti S, Hogenbirk M, Dijkgraaf F, Visser L, Hoekstra M, Song J-Y, Jacobs H, Haanen J, Schumacher T. Skin-resident memory $CD8^+$ T cells trigger a state of tissue-wide pathogen alert. Science 346, 101–105 (2014). [PubMed: 25278612]
10. Ma C, Mishra S, Demel EL, Liu Y, Zhang N. TGF-β controls the formation of kidney-resident T cells via promoting Eeffector T cell extravasation. J. Immunol 198, 749–756 (2017). [PubMed: 27903738]
11. Mackay LK, Wynne-Jones E, Freestone D, Pellicci DG, Mielke LA, Newman DM, Braun A, Masson F, Kallies A, Belz GT, Carbone FR. T-box transcription factors combine with the

cytokines TGF-β and IL-15 to control tissue-resident memory T cell fate. Immunity 43, 1101–11 (2015). [PubMed: 26682984]

12. Schenkel JM, Fraser KA, Casey KA, Beura K, Pauken KE, Vezys V, Masopust D. IL-15−Independent maintenance of tissue-resident and boosted effector memory CD8 T cells. J. Immunol 196, 3920–3926 (2016). [PubMed: 27001957]
13. Mackay LK, Rahimpour A, Ma JZ, Collins N, Stock AT, Hafon M-L, Vega-Ramos J, Lauzurica P, Mueller SN, Stefanovic T, Tscharke DC, Heath WR, Inouye M, Carbone FR, Gebhardt T. The developmental pathway for $CD103^{+}CD8^{+}$ tissue-resident memory T cells of skin. Nat. Immunol 14, 1294–1301 (2013). [PubMed: 24162776]
14. Skon CN, Lee J-Y, Anderson KG, Masopust D, Hogquist KA, Jameson SC. Transcriptional downregulation of S1pr1 is required for the establishment of resident memory $CD8^{+}$ T cells. Nat. Immunol 14, 1285–93 (2013). [PubMed: 24162775]
15. Khan TN, Mooster JL, Kilgore AM, Osborn JF, Nolz JC. Local antigen in nonlymphoid tissue promotes resident memory $CD8^{+}$ T cell formation during viral infection. J. Exp. Med 213, 951–966 (2016). [PubMed: 27217536]
16. Hombrink P, Helbig C, Backer RA, Piet B, Oja AE, Stark R, Brasser G, Jongejan A, Jonkers RE, Nota B, Basak O, Clevers HC, Moerland PD, Amsen D, van Lier RAW. Programs for the persistence, vigilance and control of human $CD8^{+}$ lung-resident memory T cells. Nat. Immunol 17, 1467–1478 (2016). [PubMed: 27776108]
17. Muschaweckh A, Buchholz VR, Fellenzer A, Hessel C, König PA, Tao S, Tao R, Heikenwälder M, Busch DH, Korn T, Kastenmüller W, Drexler I, Gasteiger G. Antigen-dependent competition shapes the local repertoire of tissue-resident memory $CD8^{+}$ T cells. J. Exp. Med 213, 3075–3086 (2016). [PubMed: 27899444]
18. Casey KA, Fraser KA, Schenkel JM, Moran A, Abt MC, Beura LK, Lucas PJ, Artis D, Wherry EJ, Hogquist K. Antigen independent differentiation and maintenance of effector-like resident memory T cells in tissues. J. Immunol 188, 612–625 (2013).
19. Graham JB, Da Costa A, Lund JM. Regulatory T cells shape the resident memory T cell response to virus infection in tissues. J. Immunol 192, 683–690 (2014). [PubMed: 24337378]
20. Mockus TE, Shwetank, Lauver MD, Ren HM, Netherby CS, Salameh T, Kawasawa YI, Yue F, Broach JR, Lukacher AE. CD4 T cells control development and maintenance of brain-resident CD8 T cells during polyomavirus infection. PLoS Pathog 14, e1007365 (2018). [PubMed: 30372487]
21. Cullen JG, Mcquilten HA, Quinn KM, Olshansky M, Russ BE, Morey A, Wei S, Prier JE, La NL, Doherty PC, Turner SJ. $CD4^{+}$ T help promotes influenza virus-specific $CD8^{+}$ T cell memory by limiting metabolic dysfunction. Proc. Natl. Acad. Sci. (USA) 116, 4481–88 (2019). [PubMed: 30787194]
22. Hwang S, Cobb DA, Bhadra R, Youngblood B, Khan IA. Blimp-1–mediated CD4 T cell exhaustion causes CD8 T cell dysfunction during chronic toxoplasmosis. J. Exp. Med 213, 1799–1818 (2016). [PubMed: 27481131]
23. Steinbach K, Vincenti I, Kreutzfeldt M, Page N, Muschaweckh A, Wagner I, Drexler I, Pinschewer D, Korn T, Merkler D. Brain-resident memory T cells represent an autonomous cytotoxic barrier to viral infection. J. Exp. Med 213, 1571–87 (2016). [PubMed: 27377586]
24. Carson K, Focosi D, Major E, Petrini M, Richey E, West D, Bennett C. Monoclonal antibody-associated progressive multifocal leucoencephalopathy in patients treated with rituximab, natalizumab, and efalizumab: a Review from the Research on Adverse Drug Events and Reports (RADAR) Project. Lancet Oncol 10, 816–824 (2009). [PubMed: 19647202]
25. Molloy ES, Calabrese LH. Progressive Multifocal Leukoencephalopathy A national estimate of frequency in systemic lupus erythematosus and other rheumatic diseases. Arthritis Rheum 60, 3761–3765 (2009). [PubMed: 19950261]
26. Van Assche G, Van Ranst M, Sciot R, Dubois B, Vermeire S, Norman M, Verbeeck J, Geboes K, Robberecht W, Rutgeerts P. Progressive multifocal leukoencephalopathy after natalizumab therapy for Crohn's disease. N. Engl. J. Med 353, 362–368 (2005). [PubMed: 15947080]
27. Casey KA, Mescher MF. IL-21 promotes differentiation of naive CD8 T cells to a unique effector phenotype. J. Immunol 178, 7640–48 (2007). [PubMed: 17548600]

28. Novy P, Huang X, Leonard WJ, Yang Y. Intrinsic IL-21 signaling is critical for CD8 T cell survival and memory formation in response to vaccinia viral infection. J. Immunol 186, 2729–38 (2011). [PubMed: 21257966]
29. Cui W, Liu Y, Weinstein JS, Craft J, Kaech SM. An interleukin-21-interleukin-10-STAT3 pathway is critical for functional maturation of memory $CD8^+$ T Cells. Immunity 35, 792–805 (2011). [PubMed: 22118527]
30. Tian Y, Cox MA, Kahan SM, Ingram JT, Rakesh K, Zajac AJ. A context-dependent role for IL-21 in modulating the differentiation, distribution, and abundance of effector and memory CD8 T cell subsets. J. Immunol 196, 2153–66 (2016). [PubMed: 26826252]
31. Phares TW, Stohlman SA, Hwang M, Min B, Hinton DR, Bergmann CC. CD4 T cells promote CD8 T cell immunity at the priming and effector site during viral encephalitis. J. Virol 86, 2416–2427 (2012). [PubMed: 22205741]
32. Phares TW, Disano KD, Hinton DR, Hwang M, Zajac AJ, Stohlman SA, Bergmann CC. IL-21 optimizes T cell and humoral responses in the central nervous system during viral encephalitis. J. Neuroimmunol 263, 43–54 (2013). [PubMed: 23992866]
33. Stumhofer JS, Silver JS, Hunter CA. IL-21 is required for optimal antibody production and T cell responses during chronic Toxoplasma gondii infection. PLoS One 8, e62889 (2013). [PubMed: 23667536]
34. Yi JS, Du M, Zajac AJ. A vital role for IL-21 in the control of a chronic viral infection. Science 324, 1572–76 (2009). [PubMed: 19443735]
35. Fröhlich A, Kisielow J, Schmitz I, Freigang S, Shamshiev AT, Weber J, Marsland BJ, Oxenius A, Kopf M. IL-21R on T cells is critical for sustained functionality and control of chronic viral infection. Science 324, 1576–1580 (2009). [PubMed: 19478140]
36. Elsaesser H, Sauer K, Brooks DG. IL-21 is required to control chronic viral infection. Science 324, 1569–1572 (2009). [PubMed: 19423777]
37. Lin E, Kemball CC, Hadley A, Wilson JJ, Hofstetter AR, Pack CD, Lukacher AE. Heterogeneity among viral antigen-specific $CD4^+$ T cells and their de novo recruitment during persistent polyomavirus infection. J. Immunol 185, 1692–1700 (2010). [PubMed: 20622115]
38. Frost EL, Kersh AE, Evavold BD, Lukacher AE. Cutting Edge: Resident memory CD8 T cells express high-affinity TCRs. J. Immunol 195, 1501521 (2015).
39. Marnik EA, Wang X, Sproule TJ, Park G, Gregory J, Lane-reticker SK, Jain S, Duffy T, Carter GW, Iii HCM, Roopenian DC, Christianson GJ, Lane-reticker SK, Jain S, Duffy T, Wang H, Carter GW, Morse HC III, Roopenian DC. Precocious interleukin 21 expression in naïve mice identifies a natural helper cell population in autoimmune disease. Cell Rep 21, 208–221 (2017). [PubMed: 28978474]
40. Sabatino JJ, Huang J, Zhu C, Evavold BD. High prevalence of low affinity peptide–MHC II tetramer–negative effectors during polyclonal $CD4^+$ T cell responses. J. Exp. Med 208, 81–90 (2011). [PubMed: 21220453]
41. Martinez RJ, Andargachew R, Martinez HA, Evavold BD. Low-affinity $CD4^+$ T cells are major responders in the primary immune response. Nat. Commun 7, 13848 (2016). [PubMed: 27976744]
42. Stubbington MJT, Mahata B, Svensson V, Deonarine A, Nissen JK, Betz AG, Teichmann SA. An atlas of mouse $CD4^+$ T cell transcriptomes. Biol. Direct 10 (2015), doi:10.1186/s13062-015-0045-x.
43. Weinstein JS, Lezon-geyda K, Maksimova Y, Craft S, Zhang Y, Su M. Global transcriptome analysis and enhancer landscape of human primary T follicular helper and T effector lymphocytes. Blood 124, 3719–3729 (2014). [PubMed: 25331115]
44. Kumar BV, Ma W, Miron M, Granot T, Guyer RS, Carpenter DJ, Senda T, Sun X, Ho S-H, Lerner H, Friedman AL, Shen Y, Farber DL. Human tissue-resident memory T cells are defined by core transcriptional and functional signatures in lymphoid and mucosal sites. Cell Rep 20, 2921–2934 (2017). [PubMed: 28930685]
45. Beura LK, Fares-Frederickson NJ, Steinert EM, Scott MC, Thompson EA, Fraser KA. $CD4^+$ resident memory T cells dominate immunosurveillance and orchestrate local recall responses. J. Exp. Med 216, 1214–1229 (2019). [PubMed: 30923043]

46. Subramanian A, Tamayo P, Mootha VK, Mukherjee S, Ebert BL, Gillette MA, Paulovich A, Pomeroy SL, Golub TR, Lander ES, Mesirov JP. Gene set enrichment analysis: A knowledge-based approach for interpreting genome-wide expression profiles. Proc. Natl. Acad. Sci. (USA) 102, 15545–15550 (2005). [PubMed: 16199517]
47. Mootha VK, Lindgren CM, Eriksson KF, Subramanian A, Sihag S, Lehar J, Puigserver P, Carlsson E, Ridderstråle M, Laurila E, Houstis N, Daly MJ, Patterson N, Mesirov JP, Golub TR, Tamayo P, Spiegelman B, Lander ES, Hirschhorn JN, Altshuler D, Groop LC. PGC-1α-responsive genes involved in oxidative phosphorylation are coordinately downregulated in human diabetes. Nat. Genet 34, 267–273 (2003). [PubMed: 12808457]
48. Effector I-IS, Cells CDT, Noguchi N, Nakamura R, Hatano S, Yamada H, Sun X, Ohara N. Interleukin-21 induces short-lived effector CD8$^+$ T cells but does not inhibit their exhaustion after Mycobacterium bovis BCG infection in mice. Infect. Immun 86, e00147–18 (2018). [PubMed: 29844233]
49. Zhou Y, Zhou B, Pache L, Chang M, Khodabakhshi AH, Tanaseichuk O, Benner C, Chanda SK. Metascape provides a biologist-oriented resource for the analysis of systems-level datasets. Nat. Commun 10 (2019), doi:10.1038/s41467-019-09234-6.
50. Leger AJ St., Jeon S, Hendricks RL. Broadening the repertoire of functional Herpes Simplex Virus Type 1−specific CD8$^+$ T cells reduces viral reactivation from latency in sensory ganglia. J. Immunol 191, 2258–2265 (2013). [PubMed: 23878317]
51. Geltink RIK, Kyle RL, Pearce EL. Unraveling the complex interplay between T cell metabolism and function. Annu. Rev. Immunol 36, 461–488 (2018). [PubMed: 29677474]
52. Konjar Š, Veldhoen M. Dynamic metabolic state of tissue resident CD8 T cells. Front. Immunol 10, 1683 (2019). [PubMed: 31379871]
53. Ditoro D, Winstead CJ, Pham D, Witte S, Andargachew R, Singer JR, Wilson CG, Zindl CL, Luther RJ, Silberger DJ, Weaver BT, Kolawole EM, Martinez RJ, Turner H, Hatton RD, Moon JJ, Way SS, Evavold BD, Weaver CT. Differential IL-2 expression defines developmental fates of follicular versus nonfollicular helper T cells. Science 361, eaao2933 (2018). [PubMed: 30213884]
54. Pepper M, Pagán AJ, Igyártó BZ, Taylor JJ, Jenkins MK. Opposing signals from the Bcl6 transcription factor and the interleukin-2 receptor generate T helper 1 central and effector Memory Cells. Immunity 35, 583–595 (2011). [PubMed: 22018468]
55. Khanna KM, Bonneau RH, Kinchington PR, Hendricks RL. Herpes simplex virus-specific memory CD8$^+$ T cells are selectively activated and retained in latently infected sensory ganglia. Immunity 18, 593–603 (2003). [PubMed: 12753737]
56. Gasnault J, Kahraman M, De Herve MGDG, Durali D, Delfraissy JF, Taoufik Y. Critical role of JC virus-specific CD4 T-cell responses in preventing progressive multifocal leukoencephalopathy. AIDS 17, 1443–1449 (2003). [PubMed: 12824781]
57. Gheuens S, Bord E, Kesari S, Simpson DM, Gandhi RT, Clifford DB, Berger JR, Ngo L, Koralnik IJ. Role of CD4$^+$ and CD8$^+$ T-cell responses against JC virus in the outcome of patients with progressive multifocal leukoencephalopathy (PML) and PML with immune reconstitution inflammatory syndrome. J. Virol 85, 7256–7263 (2011). [PubMed: 21543472]
58. Dubois E, Ruschil C, Bischof F. Low frequencies of central memory CD4 T cells in progressive multifocal Leukoencephalopathy. Neurol. Neuroimmunol. NeuroInflammation 2, e177 (2015).
59. Delgoffe GM, Powell JD. Feeding an army: the metabolism of T cells in activation, anergy, and exhaustion. Mol Immunol 68, 492–496 (2015). [PubMed: 26256793]
60. Pan Y, Kupper TS, Walsh CM. Metabolic reprogramming and longevity of tissue-resident memory T cells. Front. Immunol 9, 1347 (2018). [PubMed: 29967608]
61. Sullivan DO, Van Der Windt GJW, Huang SC, Curtis JD, Chang C, Buck MD, Qiu J, Smith AM, Lam WY, Diplato LM, Hsu F, Birnbaum MJ, Pearce EJ, Pearce EL. Memory CD8$^+$ T cells use cell-intrinsic lipolysis to support the metabolic programming necessary for development. Immunity 41, 75–88 (2014). [PubMed: 25001241]
62. Pan Y, Tian T, Park CO, Lofftus SY, Mei S, Liu X, Luo C, O'Malley JT, Gehad A, Teague JE, Divito SJ, Fuhlbrigge R, Puigserver P, Krueger JG, Hotamisligil GS, Clark RA, Kupper TS. Survival of tissue-resident memory T cells requires exogenous lipid uptake and metabolism. Nature 543, 252–256 (2017). [PubMed: 28219080]

63. Scharping NE, Menk AV, Moreci RS, Watkins SC, Ferris RL, Delgoffe GM, Scharping NE, Menk AV, Moreci RS, Whetstone RD, Dadey RE. The tumor microenvironment represses T cell mitochondrial biogenesis to drive intratumoral T cell metabolic insufficiency and dysfunction. Immunity 45, 374–388 (2016). [PubMed: 27496732]
64. Lin R, Zhang H, Yuan Y, He Q, Zhou J, Li S, Sun Y, Li DY, Qiu H, Wang W, Zhuang Z, Chen B, Huang Y, Liu C, Wang Y, Cai S, Ke Z, He W. Fatty acid oxidation controls $CD8^+$ tissue-resident memory T-cell survival in gastric adenocarcinoma. Cancer Immunol. Res 8, 479–492 (2020). [PubMed: 32075801]
65. Pan Y, Tian T, Park CO, Lofftus SY, Mei S, Liu X, Luo C, Malley JTO, Gehad A, Teague JE, Divito SJ, Fuhlbrigge R, Puigserver P, Krueger JG, Hotamisligil GS, Clark RA, Kupper TS. Survival of tissue-resident memory T cells requires exogenous lipid uptake and metabolism. Nat. Publ. Gr 543, 252–256 (2017).
66. Romano A, Koczwara JB, Gallelli CA, Vergara D, Micioni Di Bonaventura MV, Gaetani S, Giudetti AM. Fats for thoughts: An update on brain fatty acid metabolism. Int. J. Biochem. Cell Biol 84, 40–45 (2017). [PubMed: 28065757]
67. Loschinski R, Böttcher M, Stoll A, Bruns H, Mackensen A, Mougiakakos D. IL-21 modulates memory and exhaustion phenotype of T-cells in a fatty acid oxidation-dependent manner. Oncotarget 9, 13125–13138 (2018). [PubMed: 29568345]
68. Berger J. JCV-specific CD4 T cell response: another piece of the puzzle in explaining some aspects of AIDS associated PML. AIDS 17, 1557–9 (2003). [PubMed: 12824794]
69. Ozaki K, Spolski R, Feng CG, Qi C, Cheng J, Sher A, Iii HCM, Liu C, Schwartzberg PL, Leonard WJ. A Critical Role for IL-21 in Regulating Immunoglobulin Production. Science 298, 1630–1635 (2002). [PubMed: 12446913]
70. Reinhardt RL, Liang HE, Locksley RM. Cytokine-secreting follicular T cells shape the antibody repertoire. Nat. Immunol 10, 385–393 (2009). [PubMed: 19252490]
71. DeVos SL, Miller TM. Direct intraventricular delivery of drugs to the rodent central nervous system. J. Vis. Exp 75, e50326 (2013).
72. Kemball CC, Lee EDH, Vezys V, Pearson TC, Larsen CP, Aron E, Kemball CC, Lee EDH, Vezys V, Pearson TC, Larsen CP, Lukacher AE. Late priming and variability of epitope-specific $CD8^+$ T cell responses during a persistent virus infection. J. Immunol 174, 7950–7960 (2005). [PubMed: 15944301]
73. Anderson KG, Mayer-Barber K, Sung H, Beura L, James BR, Taylor JJ, Qunaj L, Griffith TS, Vezys V, Barber DL, Masopust D. Intravascular staining for discrimination of vascular and tissue leukocytes. Nat. Protoc 9, 209–222 (2014). [PubMed: 24385150]
74. Kolawole EM, Andargachew R, Liu B, Jacobs JR, Evavold BD. 2D kinetic analysis of TCR and CD8 coreceptor for LCMV GP33 epitopes. Front. Immunol 9, 2348 (2018). [PubMed: 30374353]

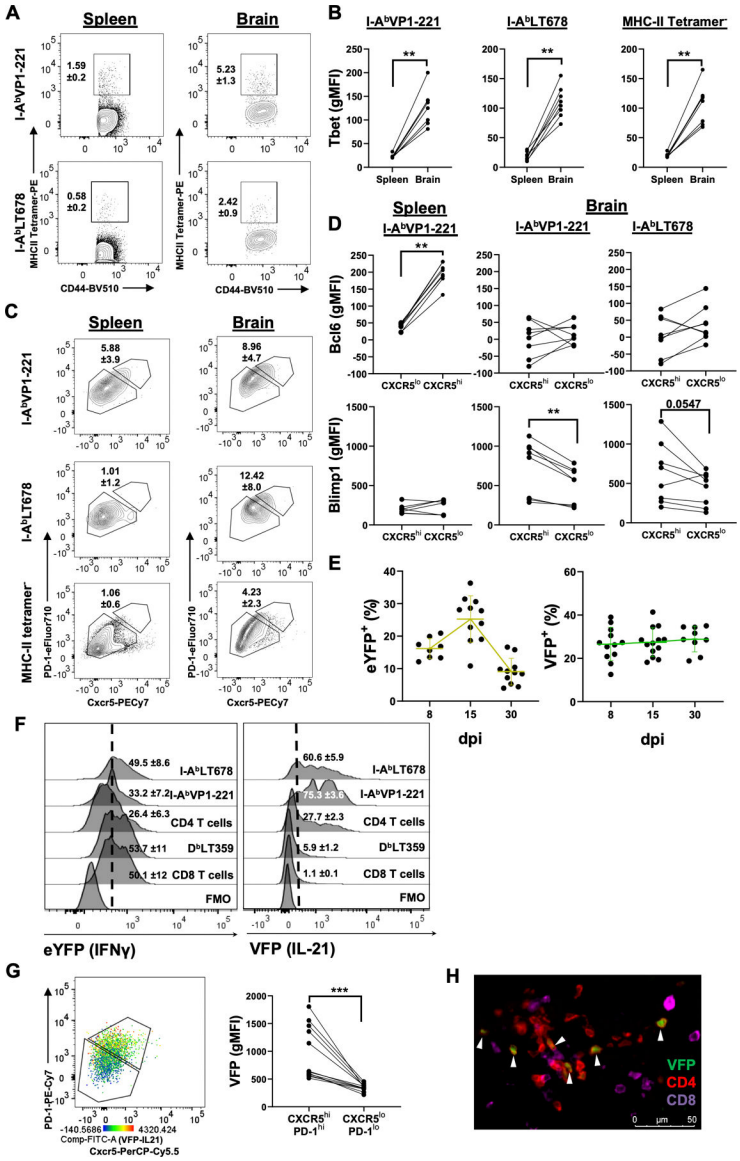

Fig. 1. CXCR5^{hi} PD-1^{hi} MuPyV-specific CD4 T cells in the brain produce IL-21.

(**A**) Representative dot plots with mean ±SD of the MuPyV CD4 epitopes I-A^b VP1–221 (**top**) and I-A^b LT678 (**bottom**) from the spleens (**left**) and brains (**right**). Gates were drawn using I-A^b CLIP tetramer controls. (**B**) gMFI of T-bet in the I-A^b VP1–221$^+$ (**left**), I-A^b LT678$^+$ (**center**) or MHC-II tetramer$^-$ (**right**) CD4 T cells from spleens and brains. (**C**) Representative plots of the indicated MHC-II tetramer$^+$ and MHC-II tetramer$^-$ populations showing PD-1 and CXCR5. Mean ±SD of CXCR5^{hi}PD-1^{hi} population shown. (**D**) gMFI of Bcl6 (**top**) and Blimp1 (**bottom**) in the CXCR5^{hi}PD-1^{hi} (CXCR5^{hi}) and CXCR5$^{int\text{-}lo}$PD-1$^{int\text{-}lo}$ (CXCR5^{lo}) populations gated on in (**A**) for I-A^b VP1–221$^+$ and I-A^b LT678$^+$ CD4 T cells from the spleens and/or brains (**E**) % CD4 T cells that are eYFP$^+$ (**left**) or VFP$^+$ (**right**) from IFNγ-eYFP and IL21-VFP reporter mice respectively, at 8, 15, and 30 dpi. (Indicate what error bars represent) (**F**) Representative histograms with mean ±SD showing eYFP (**left**) and VFP (**right**) in the indicated cells isolated from the brains of IFNγ-

eYFP or IL21-VFP reporter mice, respectively. (**G**) Representative dot plot (**left**) of total CD4 T cells from the brain of IL21-VFP reporter mice plotted for PD-1 vs. CXCR5 with VFP expression in each individual cell displayed on a blue (low) to red (high) scale, and gMFI of VFP in each gated population (**right**). (**H**) Fluorescence micrograph of CD4 (red), IL21-VFP (green) and CD8 (purple). White arrowheads point to VFP^+ CD4 T cells. **Statistics:** (**B**), (**D**) & (**G**) Wilcoxon signed-rank test. $^{**}p \leq 0.01$ $^{***}p \leq 0.005$. Data not significant unless noted. All data are from 2–3 independent experiments (n = 10–21 mice/group) using MuPyV-infected mice at 15 dpi unless noted.

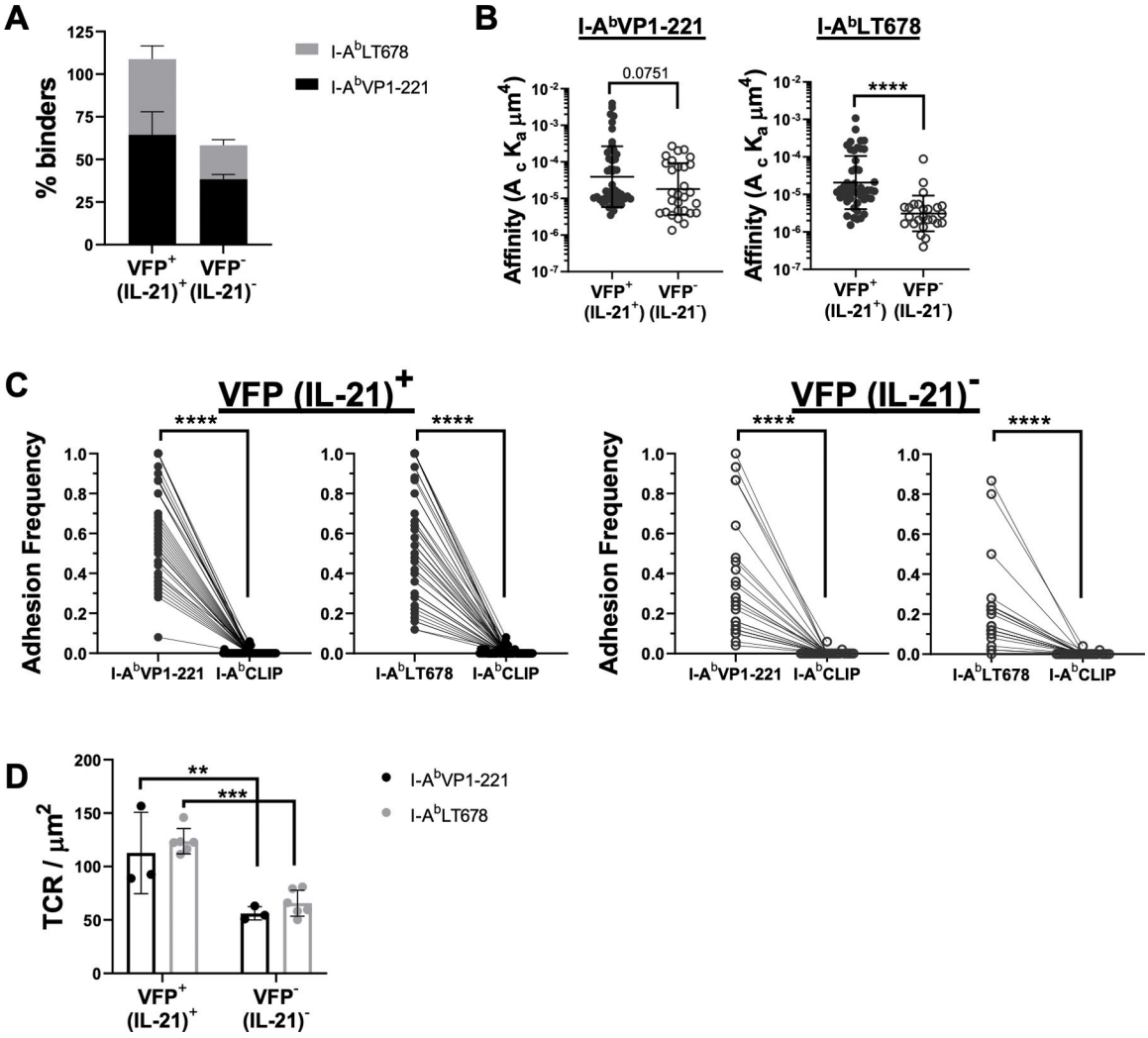

Fig. 2. IL-21-producing MuPyV-specific CD4 T cells in the brain express high-affinity TCRs.

(**A**) % VFP$^+$ and VFP$^-$ CD69$^+$ brain CD4 T cells that bind I-A^b VP1–221 or I-A^b LT678 monomer-coated RBCs but not the hCLIP monomer controls, determined by 2D-MP. (**B**) TCR:pMHC affinity measurements of VFP$^+$ and VFP$^-$ brain CD4 T cells that bound I-A^{b}VP1–221 (**left**) or I-A^b LT678 (**right**) monomers. Each dot represents one cell. (**C**) Adhesion frequency of VFP$^+$ (**left**) or VFP$^-$ (**right**) pMHC-binding CD69$^+$ CD4 T cells tested against hCLIP monomers. (**D**) TCR density (number of TCRs/µm^2 of T cell surface) in VFP$^+$ and VFP$^-$ brain I-A^b VP1–221- and I-A^b LT678-specific CD4 T cells. **Statistics:** (**B**) Mann-Whitney test; (**C**) Wilcoxon signed rank test; (**D**) Two-way ANOVA with multiple comparisons. **$p \leq 0.01$ ***$p \leq 0.005$ ****$p \leq 0.001$. All data from IL21-VFP reporter mice (n = 9–12 mice/group) at 15 dpi from two independent experiments.

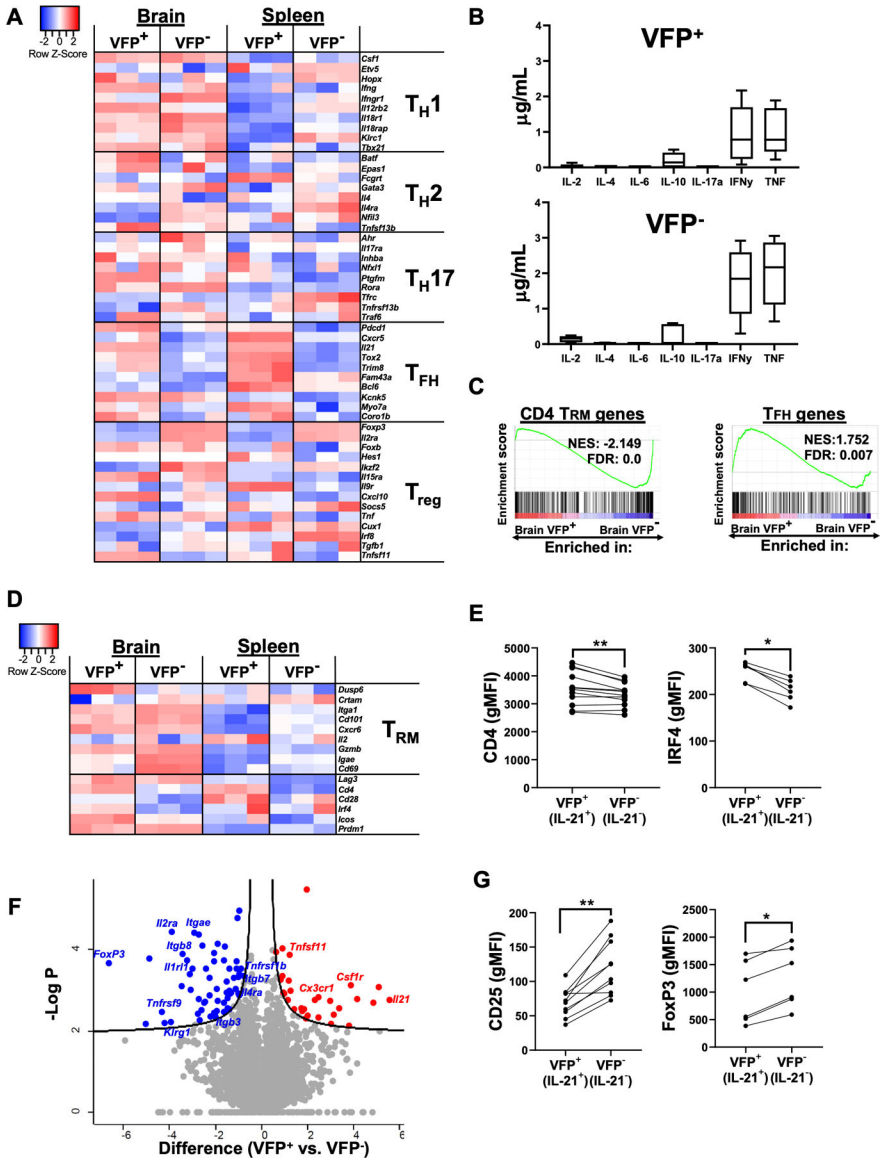

Fig. 3. IL-21-producing CD4 T cells in the brain express T_H1 and T_{FH} transcriptomes.

(**A**) Heatmap of $\log_2$ transformed RPKM values for the top genes associated with the indicated CD4 T cell subsets in $CD69^+VFP^+$ and $CD69^+VFP^-$ CD4 T cells from brains and spleens. (**B**) CBA for cytokines secreted by VFP^+ (**top**) and VFP^- (**bottom**) brain CD4 T cells after CD3/CD28 dynabead stimulation. (**C**) GSEA comparing brain VFP^+ to VFP^- CD4 T cells using CD4 T cell T_{RM} (45) (**left**) and T_{FH} (43) (**right**) gene sets. (**D**) Heatmap of $\log_2$ transformed RPKM values for the indicated genes in $CD69^+VFP^+$ and $CD69^+VFP^-$ CD4 T cells from brains and spleens. (**E**) gMFI of CD4 (**left**) and IRF4 (**right**) on brain VFP^+ and VFP^- CD4 T cells. (**F**) Volcano plot of genes differentially expressed in brain VFP^+ vs. VFP^- CD4 T cells. (**G**) gMFI of CD25 (**top**) and FoxP3 (**bottom**) expression in brain VFP^+ and VFP^- CD4 T cells. **Statistics:** (**E**) & (**G**): Wilcoxon signed rank test. $*p \leq 0.05$ $**p \leq 0.01$. (**A**), (**C**), (**D**), & (**F**) acquired from 3 separate sample pools of 4–5 IL21-VFP

reporter mice at 15 dpi. All other data are from IL21-VFP reporter mice (n = 12–14 mice/group) at 15 dpi from two independent experiments.

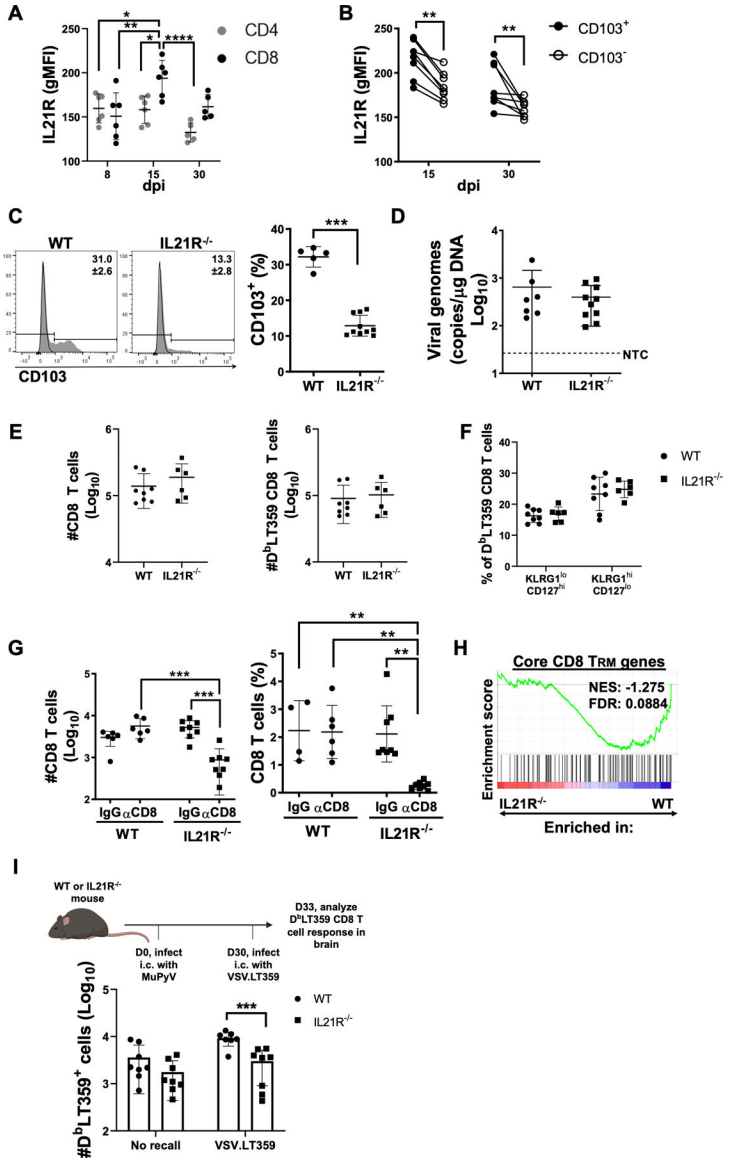

Fig. 4. CD8 T cells require IL-21 signaling to become brain-resident memory T cells.

(**A**) IL21R gMFI on CD4 and CD8 T cells from brains of WT mice at the indicated dpi. (**B**) IL21R gMFI on $CD103^+$ and $CD103^-$ brain D^b $LT359^+$ CD8 T cells at 15 and 30 dpi. (**C**) Representative histograms of CD103 on D^b $LT359^+$ CD8 T cells from brains of WT and $IL21R^{-/-}$ mice (**left**). Black line traces the FMO used to assign the indicated gates. Mean ±SD of % $CD103^+$ in upper right corner. % $CD103^+$ D^b $LT359^+$ brain CD8 T cells from WT and $IL21R^{-/-}$ mice (**right**). (**D**) qPCR for MuPyV DNA in the brains of WT and $IL21R^{-/-}$ mice. NTC= no template control. (**E**) Number of total and D^b $LT359^+$ CD8 T cells from brains of WT and $IL21R^{-/-}$ at 8 dpi. (**F**) KLRG1 and CD127 expression pattern by brain D^b $LT359^+$ CD8 T cells of WT and $IL21R^{-/-}$ mice at 8 dpi. (**G**) Number (**left**) and % CD8 T cells (**right**) in brains of MuPyV-infected mice given IgG or anti-CD8β. (**H**) GSEA comparing brain CD8 T cells from $IL21R^{-/-}$ vs. WT mice using a core T_{RM} signature gene set (5). (**I**) Experimental design (**above**) and number of D^b $LT359^+$ CD8 T cells after

rechallenge with VSV.LT359 in WT and IL21R$^{-/-}$ mice. **Statistics:** (**A**), (**G**), & (**I**): Two-way ANOVA with multiple comparisons; (**B**) Wilcoxon test. (**C**)-(**F**): Mann-Whitney test. *$p \leq 0.05$, **$p \leq 0.01$, ***$p \leq 0.005$, ****$p \leq 0.001$. Data is not significant unless noted. (**H**) data acquired from 3 separate pools of brain D^b LT359$^+$ CD8 T cells sorted from WT and IL21R$^{-/-}$ mice (n = 4–5 mice/group) at 30 dpi. All other data from 2–3 independent experiments with 2–5 mice per group, and at 30 dpi unless noted.

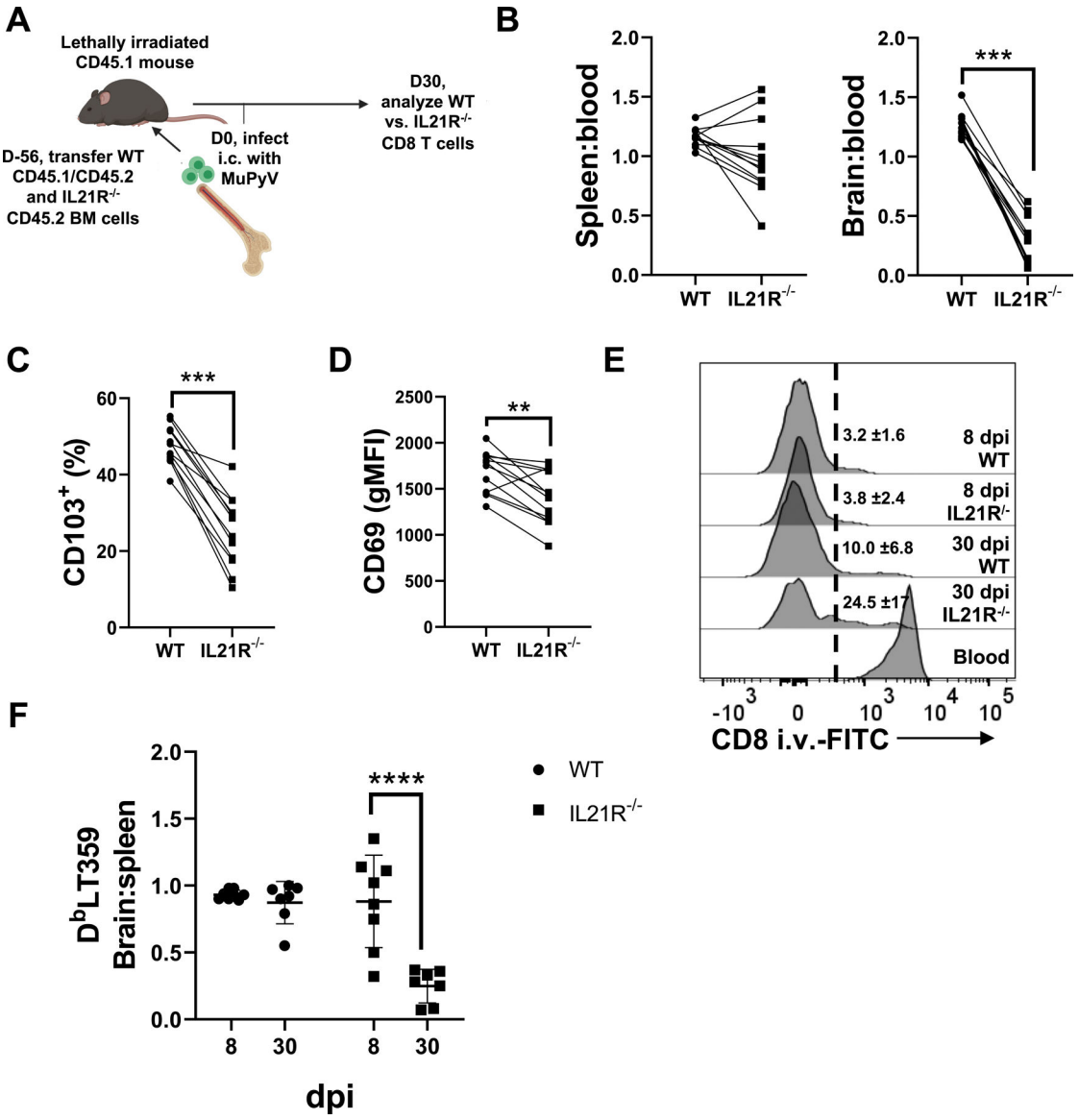

Fig. 5. IL-21 signaling for development of brain-resident memory is CD8 T cell-intrinsic.

(**A**) Experimental design. (**B**) Ratio of spleen (**left**) and brain (**right**) CD45.1$^+$/CD45.2$^+$ (WT) and CD45.2$^+$ (IL21R$^{-/-}$) CD8 T cells to blood CD45.1$^+$/CD45.2$^+$ (WT) and CD45.2$^+$ (IL21R$^{-/-}$) CD8 T cells in BM chimeras. (**C**) % CD103$^+$ cells in WT and IL21R$^{-/-}$ CD8 T cells in brain in BM chimeric mice. (**D**) gMFI of CD69 in WT and IL21R$^{-/-}$ CD8 T cells in brains of BM chimeric mice. (**E**) anti-CD8α i.v. labeling of the indicated CD8 T cell populations at 8 and 30 dpi from the brains of BM chimeric mice. (**F**) Ratio of the % brain CD45.1$^+$/CD45.2$^+$ (WT) and CD45.2$^+$ (IL21R$^{-/-}$) D^b LT359$^+$ CD8 T cells to % spleen CD45.1$^+$/CD45.2$^+$ (WT) and CD45.2$^+$ (IL21R$^{-/-}$) D^b LT359$^+$ CD8 T cells in BM chimeric mice. **Statistics:** (**B**)-(**E**) Wilcoxon test. (**G**) Two-way ANOVA with multiple comparisons. *p≤0.05, **p≤0.01, ***p≤0.005, ****p≤0.001. Data is not significant unless noted. Data are from 2–3 independent experiments with 3–4 mice per group.

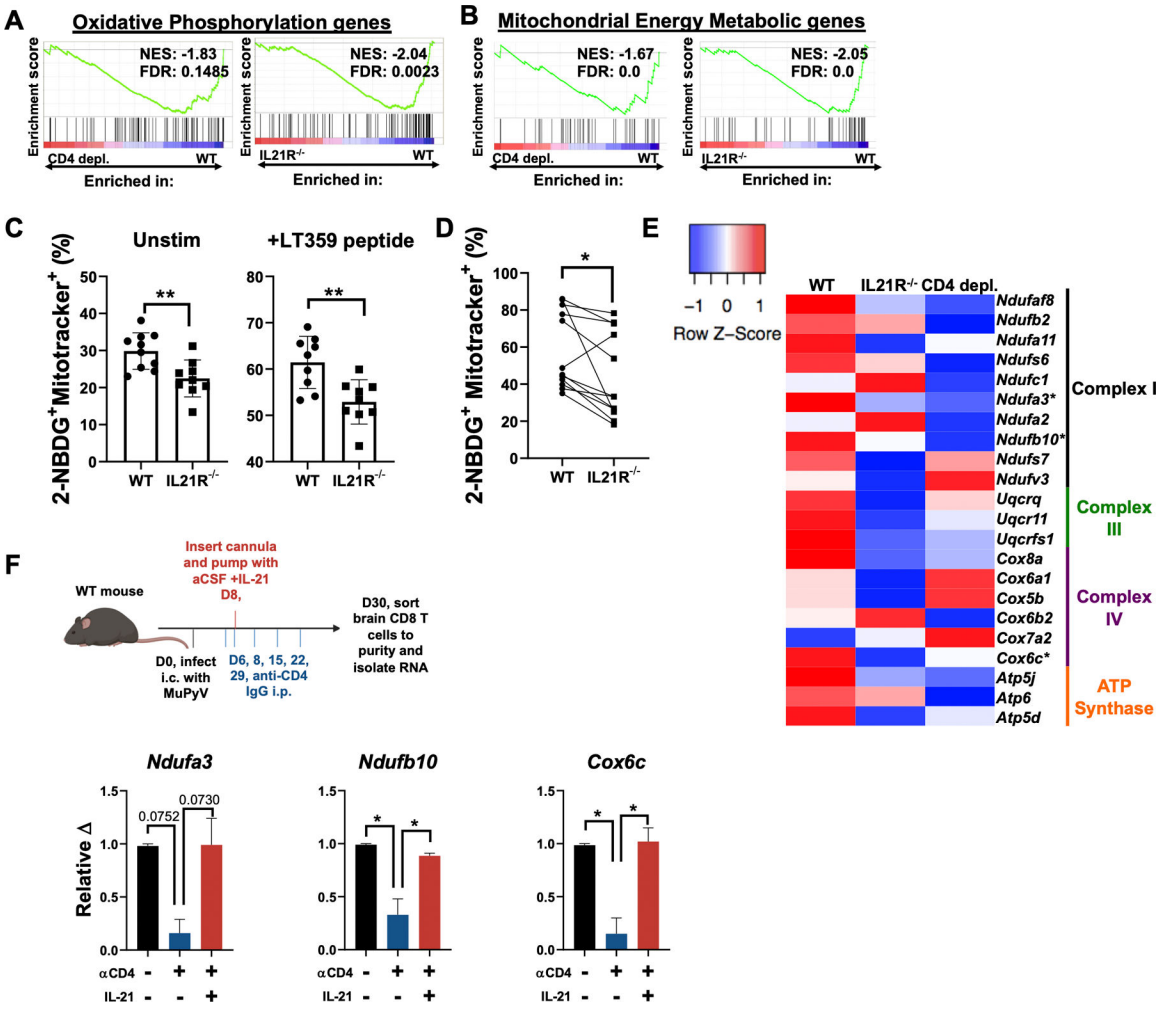

Fig. 6. IL-21 signaling controls oxidative metabolism by MuPyV-specific CD8 T cells in the brain.

(**A**) GSEA comparing CD4 T cell-depleted (CD4-depl.) vs. WT mice (**left**) and IL21R$^{-/-}$ vs. WT mice (**right**) using the KEGG oxidative phosphorylation gene set. (**B**) GSEA comparing CD4 T cell-depleted (CD4-depl.) vs. WT mice (**left**) and IL21R$^{-/-}$ vs. WT mice (**right**) using mitochondrial energy genes. (**C**) % CD8 T cells from brains of WT or IL21R$^{-/-}$ mice that incorporated 2-NBDG and Mitotracker Deep Red with (**right**) and without (**left**) LT359 peptide stimulation. (**D**) % CD8 T cells that incorporated 2-NBDG and Mitotracker Deep Red after LT359 peptide stimulation in CD8 T cells from the brains of WT/IL21R$^{-/-}$ BM chimeric mice. (**E**) Heatmap of $\log_2$ transformed RPKM read values for genes within the indicated ETC complexes. (**F**) Experimental design (**above**) and relative change of gene expression in CD8 T cells isolated from the brains of WT, CD4 T cell-depleted, and CD4 T cell-depleted + i.c.v. IL-21 treated mice for select ETC genes (**below**). **Statistics:** (**C**) Mann-Whitney test; (**D**) Wilcoxon signed rank test; (**F**) One-way ANOVA with multiple comparisons. *$p \leq 0.05$, **$p \leq 0.01$. Data is not significant unless noted. (**A**), (**B**) & (**E**) data from 2–3 separate sample pools of WT, CD4 T cell-depleted, and IL21R$^{-/-}$ mice at 30 dpi (n = 4–5 mice/group). All other data are from 2–3 independent experiments with 2–5 mice per group at 30 dpi.